

# Topology of quantum discord

Nga T. T. Nguyen and Robert Joynt

*Department of Physics, University of Wisconsin, Madison, Wisconsin 53706, USA*

Quantum discord is an important measure of quantum correlations that can serve as a resource for certain types of quantum information processing. Like entanglement, discord is subject to destruction by external noise. The routes by which this destruction can take place depends on the shape of the hypersurface of zero discord  $\mathcal{C}$  in the space of generalized Bloch vectors. For 2 qubits, we show that with a few points subtracted, this hypersurface is a simply-connected 9-dimensional manifold embedded in a 15-dimensional background space. We do this by constructing an explicit homeomorphism from a known manifold to the subtracted version of  $\mathcal{C}$ . We also construct a coordinate map on  $\mathcal{C}$  that can be used for integration or other purposes. This topological characterization of  $\mathcal{C}$  has important implications for the classification of the possible time evolutions of discord in physical models. The classification for discord contrasts sharply with the possible evolutions of entanglement. Using topological methods, we classify the possible joint evolutions of entanglement and discord. There are 9 allowed categories: 6 categories for a Markovian process and 3 categories for a non-Markovian process, respectively. We illustrate these conclusions with an anisotropic XY spin model. All 9 categories can be obtained by adjusting parameters.

PACS numbers: 03.67.Lx, 03.67.Ac, 03.65.Yz, 02.40.Pc

## I. INTRODUCTION

Some of the most characteristic features of quantum mechanics show up in the correlations of two subsystems that are independently measurable. The most famous is entanglement<sup>1</sup>, but this notion does not exhaust everything that is quantum about correlations. Even two systems that are separable have zero entanglement can violate Bayes theorem, something that cannot happen in classical physics. One quantity that measures the additional quantumness of correlations is quantum discord  $D$ <sup>2,3</sup>. Roughly speaking  $D$  is the difference between the total correlation once entanglement has been subtracted out, and the purely classical correlation. Discord can serve as a resource for the accomplishment of certain tasks in a way somewhat similar to the way that entanglement can. For computation, the quantum algorithm DQC1 does seem to use discord rather than entanglement<sup>4-6</sup>, and the same is true for dense coding<sup>7</sup>. More general statements about the uses of discord are difficult to make at this stage. Quantum discord and other quantum correlation measures have recently received an extensive review<sup>8</sup>.

One question that is of experimental importance is how quantum correlations are erased by external noise. In the case of entanglement, there is a rather rich range of possible behaviors of the time evolution of the concurrence [the function  $C(t); t \in \{0, \infty\}$ ] as a composite system loses its quantum correlations<sup>9</sup>. A somewhat similar, though distinctly more limited, range of behaviors has been found in numerical studies of the discord evolution [the function  $D(t); t \in \{0, \infty\}$ ]<sup>10-18</sup>. For entanglement, a general classification of time evolutions was seen to depend on understanding the topology of entanglement: essentially the structure of the set of separable states  $\mathcal{S}$ <sup>19,20</sup>. The

purpose of the current work is to achieve the same goal for discord. We will first determine the relevant topological properties of the set  $\mathcal{C}$  of concordant states, i.e., the set of states for which  $D$  vanishes, then deduce a general classification of the types of evolution of the discord. Furthermore, we shall give examples of physical models that realize the various types of evolution. The paper will focus on the case of 2 qubits.

The most basic result about  $\mathcal{C}$ , established by Ferraro *et al.*<sup>12</sup>, is that it is of zero 15-volume. To understand the significance of this, we first note that the set of 2-qubit density matrices, which we shall call  $\mathcal{M}$ , is a convex subset of a real 15-dimensional vector space.  $\mathcal{M}$  itself is a 15-dimensional manifold with boundary: any interior point of  $\mathcal{M}$  has a neighborhood that is homeomorphic to a neighborhood in  $\mathbb{R}^{15}$ .  $\mathcal{C}$  is a subset of  $\mathcal{M}$ . The fact that it has zero 15-volume means that the dimension of any neighborhood of any point in  $\mathcal{C}$  is less than 15, but gives no further information. We shall show that (except for one point) the precise number for the local dimensionality of  $\mathcal{C}$  is 9. It has been shown previously that  $\mathcal{C}$  is path-connected; we shall prove the stronger result that  $\mathcal{C}$  (with one point removed) is simply connected. The zero-volume statement already implies a very important point about discord evolution: sudden death of discord is not possible. This was conjectured early on from results of numerical studies and the connection with the geometry of  $\mathcal{S}$  was understood. Other phenomena, such as frozen discord<sup>11</sup>, have also been shown to benefit from a geometric analysis<sup>21</sup>. These analyses have been carried out in the 3-dimensional set of Bell-diagonal states.

Our aim here is to extend this framework to the full 15-dimensional space. This will allow us to characterize in a topological fashion all joint evolutions of entanglement and discord that lead to the disappearance of both. Some evolutions have been computed by previous authors<sup>22,23</sup>.

The paper is organized as follows: Sec. II establishes concepts and notation. Sec. III establishes the basic facts about the geometrical and topological nature of  $\mathcal{C}$ . Sec. III applies the results of Sec. II to the dynamical evolution of the discord, first establishing a categorization of the possible evolutions, then illustrating this categorization. In Sec. IV we give a discussion and the outlook for future work.

## II. DISCORD, GEOMETRIC DISCORD, AND FROZEN DISCORD

The definition of quantum discord that best expresses its foundation in information theory is:

$$D(B|A) = I(A : B) - J(B|A),$$

where  $I(A : B)$  is the quantum mutual information:

$$I(A : B) = S(A) + S(B) - S(A, B),$$

$S(A)$  is the usual von Neumann entropy, while  $J(B|A)$  is a measure of the total classical correlation present.  $J(B|A)$  is defined in stages. First note that if system  $A$  is measured by an operator  $E_a$  and is found to be in the state  $a$ , then the density matrix of  $B$  after the measurement is  $\rho(B|a) = \text{Tr}_A(E_a \rho_{AB}) / p_a$ , where  $p_a$  is the probability of measuring the result  $a$  in the state  $\rho_{AB}$ , i.e.,  $p_a = \text{Tr}(E_a \rho_{AB})$ . We may then define a conditional entropy under the measurement of  $E_a : S(B|E_a) = \sum_a p_a S(\rho_{B|a})$ , and then we have a corresponding mutual-information-like quantity  $J(B|E_a) = S(B) - S(B|E_a)$ . Quantum mechanics is distinguished from classical mechanics by the fact that this quantity depends on the choice of measurements. To remove this ambiguity, we maximize over the choice of  $\{E_a\}$  and arrive at a measure of the total classical correlation  $J(B|A) = \max_{\{E_a\}} J(B|E_a)$ .  $D(B|A)$  is clearly not symmetric between systems  $A$  and  $B$ , but it has the essential property of being invariant under local unitary operations.

For our purposes, its most important property of discord is that  $D(B|A) = 0$  when  $\rho_{AB}$  is classical-quantum:  $\rho_{AB} = \sum_a p_a \Pi_a \otimes \rho(B|a)$ . Here  $\{\Pi_a\}$  is any set of rank-one projectors and  $\rho(B|a)$  is the resulting partial density matrix for  $B$  if the result has been obtained from a measurement of  $A$ . This gives an explicit definition of the set  $\mathcal{C}$  of concordant states mentioned above.

We intend to investigate the topology of  $\mathcal{C}$ . To define a topology on any set requires a specification of its open subsets. A metric is the most convenient way to do this, and we will employ the metric on the set  $\mathcal{M}$  of density matrices that follows from the Hilbert-Schmidt inner product:  $(\rho, \rho') = \text{Tr}(\rho \rho')$ . To give a consistent treatment of discord, we also need a metric-based definition. Fortunately, there is the geometric discord, defined

by

$$D_G(B|A) = \min_{\chi \in \mathcal{C}} |\rho_{AB} - \chi| = \min_{\chi \in \mathcal{C}} \text{Tr} \left[ (\rho_{AB} - \chi)^2 \right], \quad (1)$$

i.e.,  $D_G(\rho_{AB})$  is the Hilbert-Schmidt distance from  $\rho_{AB}$  to the nearest point of  $\mathcal{C}$ . This differs slightly from the information-theory based definition above. We will comment on the differences below. Since we intend to com-

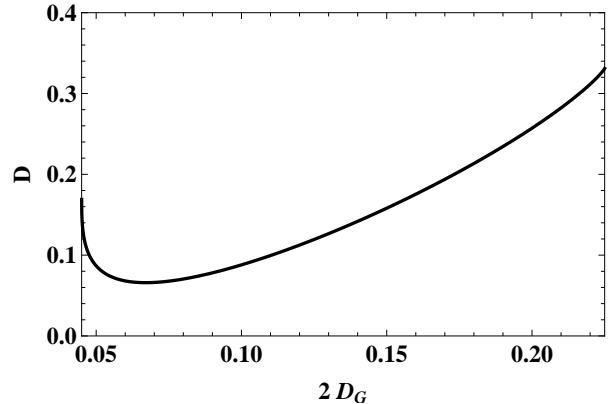


FIG. 1: The quantum discord is plotted as a function of normalized geometric discord for a trajectory that lies in the space of Bell-diagonal states. The trajectory has constant  $N_{11} = -0.7$ ,  $N_{22} = -0.3$  and  $N_{33}$  is an implicit variable along the curve. This trajectory is shown in Fig. 2. Note that a monotonically increasing  $D_G$  does not imply an increasing  $D$ .

pare entanglement and discord, we need a corresponding metrical definition of entanglement, the geometric entanglement:

$$E_G(B|A) = \min_{\chi \in \mathcal{S}} |\rho_{AB} - \chi| = \min_{\chi \in \mathcal{S}} \text{Tr} \left[ (\rho_{AB} - \chi)^2 \right],$$

where  $\mathcal{S}$  is the set of separable states, i.e.  $\rho_{AB} \in \mathcal{S}$  if and only if

$$\rho_{AB} = \sum_a p_a \rho_A^a \otimes \rho_B^a,$$

where the  $p_a$  are probabilities and  $\rho_A^a, \rho_B^a$  refer to systems  $A$  and  $B$ , respectively. We shall also have occasion to refer to classical states, which we take to be states of the form

$$\rho_{AB} = \sum_a p_a \Pi_A^a \otimes \Pi_B^a,$$

where  $\Pi_A^a, \Pi_B^a$  are projections. The set of pure states, for which there is a basis in which  $\rho_{AB}$  is itself a projection operator, will be denoted by  $\mathcal{P}$ .

For 2 qubits, a general state can be written using the basis of  $\text{SU}(4)$  generators:

$$\rho = \frac{1}{4} (\sigma_0 \otimes \sigma_0 + \sum_{i=1}^3 N_{0i} \sigma_0 \otimes \sigma_i + \sum_{i=1}^3 N_{i0} \sigma_i \otimes \sigma_0 + \sum_{i,j=1}^3 N_{ij} \sigma_i \otimes \sigma_j). \quad (2)$$

$\sigma_0$  is the  $2 \times 2$  identity and  $\sigma_{1,2,3}$  are the Pauli matrices that generate  $SU(2)$ . The 15  $SU(4)$  generators are  $\sigma_i \otimes \sigma_j$  (where either  $i > 0$  or  $j > 0$ ).  $N_{0i}$  and  $N_{i0}$  are sometimes called local Bloch vectors of qubit  $A$  and  $B$ , respectively.  $N_{ij}$  with both  $i > 0$  and  $j > 0$  is sometimes termed the correlation tensor. This representation of the density matrix is variously called the Pauli basis, the polarization vector, the coherence vector, and the generalized Bloch vector. We will usually use the latter term.

Since we will mainly use the geometric discord in this paper, it is important to clarify the distinction between the usual quantum discord and the geometric discord. Unlike a quantum entanglement measure such as the concurrence and its geometric counterpart (distance to the nearest separable state), discord and geometric discord are not always monotonic functions of one another, i.e., it is possible that  $dD/dt$  has the opposite sign from  $dD_G/dt$  at points along some trajectory  $\rho_{AB}(t)$  in the state vector space. An example is shown in Fig. 1 where quantum discord and geometric discord show different behavior for a trajectory restricted to the Bell-diagonal subclass of states defined by the fact that only the three components  $N_{11}, N_{22}, N_{33}$  are non-zero. In Fig. 1, the trajectory moves along the straight line  $N_{11} = -0.7$ ,  $N_{22} = -0.3, N_{33} = -1 + 2t$  as  $t$  varies from 0 to 1. It can be seen that there are values of  $t$  such that  $dD/dt < 0$  but  $dD_G/dt > 0$ .

The reason for this non-intuitive behavior can be seen from Fig. 2, where curves of constant  $D$  and  $D_G$  in the plane defined by  $N_{11} = -0.7$  are depicted. All allowed states then lie inside the tilted rectangle in this plane. The only concordant point in this plane is  $(N_{11}, N_{22}, N_{33}) = (-0.7, 0, 0)$  - the center of the tilted rectangle. The curves of constant geometric discord are the circles. The other more complicated curves are the curves of constant quantum discord. The trajectory of Fig. 1 is the thick vertical line segment  $N_{22} = -0.3$ , staying inside the rectangle of the vertical line plotted in Fig. 2. This trajectory hits some of the geometric discord curves only once while it hits some of the discord curves two times, which is the reason for the two different time behaviors. It is easily seen that the trajectory must be carefully chosen for this to occur, which is the reason for the arbitrary-seeming values of the trajectory parameters. One can see from this discussion that while the two quantities  $D$  and  $D_G$  measure essentially the same thing, subtle differences in the actual functional dependences mean that the relation between the two is not monotone.

### Frozen discord

“Frozen” quantum discord occurs when  $D(t)$  or  $D_G(t)$  is constant positive number for a finite interval of time. During this time period, the quantum mutual information and the classical correlations decrease, but the difference  $D = I - J_{\text{class}}$  remains fixed<sup>11,31</sup>. Since surfaces of zero discord can have simple shapes in  $N$ -space<sup>21</sup> surfaces of constant geometric discord can also have rela-

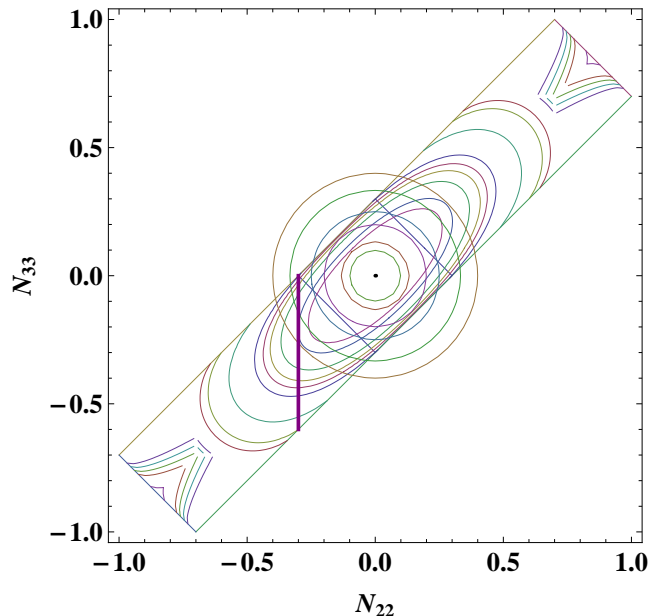


FIG. 2: (Color online) The plane of Bell-diagonal states having  $N_{11} = -0.7$ . Circles centered on the origin represent surfaces of constant geometric discord. Other more complex curves represent surfaces of constant discord. Only the states lying inside the tilted rectangle are physical states that satisfy positivity. Geometry of the Bell-diagonal subclass of states having characterized as the tilted rectangle. The square is the corresponding separable subset of this subclass of states. The larger the (geometric) discord value, the further the constant (geometric) discord curve from the concordant (zero-discord) point  $(N_{11}, N_{22}, N_{33}) = (-0.7, 0, 0)$ . The vertical line with the segment inside the rectangle describes one possible trajectory that results in discord and its geometric measure of the system not mutually monotonic increasing with one another. This is the trajectory shown in Fig. 1

tively simple shapes and simple plausible models can produce the phenomenon of frozen discord. This is much less likely to occur for the quantum discord, for which the shapes of the surfaces are typically complex. Examples of the latter are shown in Fig. 3.

## III. STATE SPACE

### A. Topology of $\mathcal{C}$

Optimizing the classical correlations requires considerable effort: closed formulas for quantum discord have been obtained only for a few classes of quantum states, typically the  $\mathbf{X}$ -type class (see e.g. Refs.<sup>24–26</sup>). The geometric discord  $D_G$ , defined in Eq. (1), is usually easier to compute. The minimization present in definition (1) can now be performed explicitly and the geometric discord is

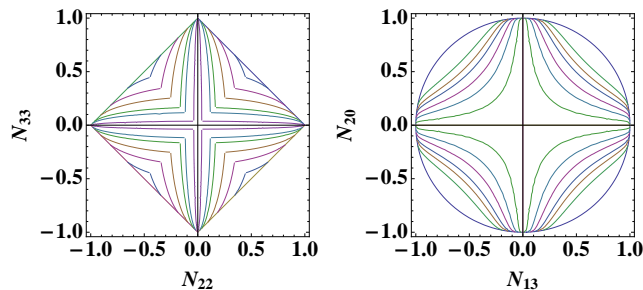


FIG. 3: (Color online) Examples of curves of constant discord for two different sections of  $N$ -space. Only the two coordinates listed are nonzero. Coordinate axes are always straight surfaces of zero discord, and discord increases as the distance from the axes increases, but the precise functional dependence varies depending on which axis pair is considered. All states inside the square and the disk are separable.

obtained in a fully analytical form<sup>27,28</sup>

$$D_G = \frac{1}{4} \left( \sum_{i=1}^3 \sum_{\alpha=0}^3 N_{i\alpha}^2 - k_{\max} \right), \quad (3)$$

where  $k_{\max}$  is the maximum eigenvalue of the matrix

$$L_{ij} = N_{i0} (N_{j0})^T + \sum_{k=1}^3 N_{ik} N_{jk}.$$

We also note that the geometric discord satisfies<sup>28,30</sup>  $1 \geq 2D_G \geq D^2$  with equality corresponding to pure states of maximally entangled.

The density matrix of the zero-discord state for a pair of qubits A and B has the form (details in appendix A):

$$\rho_{AB} = p |\Psi_0\rangle \langle \Psi_0| \otimes \rho_0 + (1-p) |\Psi_1\rangle \langle \Psi_1| \otimes \rho_1. \quad (4)$$

$\rho_k$ ,  $k = 0, 1$ , is a marginal density matrix for qubit B.  $D(\rho_{AB}) = D_G(\rho_{AB}) = 0$  if and only if  $\rho_{AB}$  has this classical-quantum form. If so, then  $\rho_{AB} \in \mathcal{C}$ , the set of concordant states.

Our goal in this section is to determine topological structure of  $\mathcal{C}$ . We shall show that if certain points are subtracted from  $\mathcal{C}$  we get a set  $\mathcal{C}_-$  that is a boundaryless 9-manifold. Thus nearly every point of  $\mathcal{C}$  has a neighborhood that is homeomorphic to an open set of  $H^9$ , the 9-dimensional half-space. This serves as a basis for understanding the dynamics of discord.

The strategy of the argument is first to establish a one-to-one continuous and invertible mapping  $f$  from a known boundaryless 9-manifold  $\mathcal{A}$  to a set  $\mathcal{C}_-$ . We then consider extensions of  $f$  in order to understand the relation of  $\mathcal{C}_-$  to  $\mathcal{C}$  itself. We can also show that the 9 tangent vectors of this mapping are linearly independent on  $\mathcal{C}_-$  so that we have a valid coordinate chart on  $\mathcal{C}_-$ . Since the difference between  $\mathcal{C}$  and  $\mathcal{C}_-$  is a set of measure zero, the coordinate chart is sufficient for purposes of, for example, integration on  $\mathcal{C}$ .

We consider the set  $\mathcal{A} = J \times S_2 \times B_3 \times B_3$ .  $\times$  denotes the Cartesian product.  $J$ , a boundaryless 1-manifold, is the open interval  $(0, 1/2)$ . Points belonging to  $J$  will be labeled by  $p$ :  $0 < p < 1/2$ .  $S_2$ , a boundaryless 2-manifold, is the 2-sphere. Points belonging to  $S_2$  will be denoted by  $\vec{m}$  or  $(m_1, m_2, m_3)$  with  $|\vec{m}|^2 = m_1^2 + m_2^2 + m_3^2 = 1$ . (Spherical polar coordinates will also be used later).  $B_3$  is the *open* 3-ball which is a boundaryless 3-manifold. Points belonging to the first copy of  $B_3$  will be denoted by  $\vec{n}_0$  or  $(n_{01}, n_{02}, n_{03})$  with  $|\vec{n}_0|^2 = n_{01}^2 + n_{02}^2 + n_{03}^2 < 1$ . Similarly for the second copy of  $B_3$  and  $\vec{n}_1$ . Since the Cartesian product of simply-connected boundaryless manifolds is a boundaryless manifold, and the dimensions add,  $\mathcal{A}$  is a simply-connected boundaryless 9-manifold. We now define a map  $f(p, \vec{m}, \vec{n}_0, \vec{n}_1)$  from  $\mathcal{A}$  to  $\mathbb{R}^{15}$  (Euclidean 15-space)  $f: \mathcal{A} \rightarrow \mathbb{R}^{15}$  by

$$N_{0i} = pm_{0i} + (1-p)n_{1i} \quad (5)$$

$$N_{i0} = (2p-1)m_i \quad (6)$$

$$N_{ij} = m_i [pn_{0j} - (1-p)n_{1j}]. \quad (7)$$

The various  $N$ 's give the 15 components (appendix A) of  $f$  and  $i, j = 1, 2, 3$ . These can be thought of as a generalized Bloch vector for states in  $\mathcal{C}$ . It contains 3 components for the marginal density matrices of the two individual qubits and 9 for the correlations. Geometrically, the points of  $N_{i0}$ , considered as a set in  $\mathbb{R}^3$ , lie on the line joining the 3-vectors  $\vec{n}_0$  and  $\vec{n}_1$ . Since  $\vec{n}_0 \in B_3$  and  $\vec{n}_1 \in B_3$ , the set of points  $N_{i0}$  (i.e., the image of  $f$  restricted to the first three dimensions of  $\mathbb{R}^{15}$ ) fills out an open 3-ball  $B_3$ , and this set is *independent of the value of  $p$* . Similarly the set of possible values of  $N_{ij}$  for any fixed  $i$  is an open 3-ball of radius  $m_i$  that is independent of  $p$ .

The physical meaning of the various parameters is clarified by computing the magnitude of  $\vec{N}$ :

$$|\vec{N}|^2 = (2p-1)^2 + 2p^2 |\vec{n}_0|^2 + 2(1-p)^2 |\vec{n}_1|^2. \quad (8)$$

Pure states have  $|\vec{N}|^2 = 3$  in our normalization, which implies that the pure states of  $\mathcal{C}$  have  $p = 0$  and  $|\vec{n}_1| = 1$ . Since entanglement and discord are the same for pure states, these are product states, as is evident if we insert the conditions for  $p$  and  $\vec{n}_1$  in Eq. (4)

$f$  consists only of polynomial functions so it is obviously smooth.  $\mathcal{C}_-$  is the image of  $f$  and it is defined by Eqs. (5), (6), (7), and the restrictions on the input variables.  $\text{im } f \subset \mathbb{R}^{15}$  and  $f$  is surjective on  $\mathcal{C}_-$  by definition.  $\mathcal{C}_-$  is clearly compact.

It remains to show that  $f$  is injective and therefore invertible. We note first from Eq. (6) that  $N_{i0}$ ,

considered as a 3-vector  $\vec{N}_0$ , lies inside a ball of radius 1:  $N_{10}^2 + N_{20}^2 + N_{30}^2 < 1$ . This follows from the fact that  $0 < 1 - 2p < 1$ . It is also the case that any point in  $\mathbb{R}^{15}$  that has  $\{N_{10}, N_{20}, N_{30}\} = \{0, 0, 0\}$  is not included in  $\mathcal{C}_-$  since  $|\vec{m}| = 1$  and  $p < 1/2$ . We will comment on this later. The restricted function  $N_{i0}(p, m_j)$  is one-to-one for all  $\{N_{10}, N_{20}, N_{30}\}$  such that  $0 < N_{10}^2 + N_{20}^2 + N_{30}^2 < 1$ , and the inverse function is  $(m_1, m_2, m_3) = (N_{10}, N_{20}, N_{30}) / |\vec{N}_0|$  and  $p = 1/2 - |\vec{N}_0|/2|\vec{m}|$ . Hence the specification of  $\vec{N}_0$  uniquely determines  $p$  and  $\vec{m}$ . Once these quantities are known and  $N_{0i}$  and  $N_{ij}$  are given, we can form the combinations

$$\begin{aligned} \frac{1}{p}(N_{0i} + N_{ij}/m_j) &= n_{0i} \\ \frac{1}{1-p}(N_{0i} - N_{ij}/m_j) &= n_{1i} \end{aligned}$$

obtained by adding and subtracting Eqs. (5) and (7). Because of the product form of  $N_{ij}$ , any choice of  $j$  for which  $m_j \neq 0$  (and at least one such must exist since  $|\vec{m}| = 1$ ) will do in these equations, which determine  $n_{0i}$  and  $n_{1i}$  uniquely. This completes the specification of  $f^{-1}$ .  $f^{-1}$  maps every point in  $\mathcal{C}_-$  to a unique point of  $\mathcal{A}$ .  $f$  is injective and  $f$  and  $f^{-1}$  are continuous, so  $f$  is a homeomorphism. Every compact subset of  $\mathcal{A}$  is mapped to a compact subset of  $\text{im } f$ , so  $f$  is an embedding and  $\mathcal{C}_-$  is a boundaryless 9-manifold. Every point in  $\mathcal{C}_-$  has a neighborhood that is homeomorphic to a neighborhood in  $\mathbb{R}^9$ .

The topology of  $\text{im } f$  is found by a parallel argument.  $\mathcal{C}_-$  is homeomorphic to  $\mathcal{A}$ , which is simply-connected since it is a Cartesian product of simply-connected manifolds. Hence  $\mathcal{C}_-$  is simply connected. Its algebraic topology is not entirely trivial, however, since the second homology group  $H_2(\mathcal{A}) = \mathbb{Z}$  (because of the factor of  $S_2$  in  $\mathcal{A}$ ), which implies that  $H_2(\mathcal{C}_-) = \mathbb{Z}$  as well.

It remains to relate  $\mathcal{C}_-$  to  $\mathcal{C}$ , the set of concordant states. To do so, we examine points in the closure of  $\mathcal{A}$  and the associated extensions of  $f$ . There are 3 classes of such points, which we now consider in turn.

1.  $|\vec{n}_0| = 1$  and  $|\vec{n}_1| = 1$ . Consider of these points to  $\mathcal{A}$  adds the boundary of  $B_3$  to the set of allowed  $N_{i0}$  and similarly for the set of allowed  $N_{ji}$  whenever  $m_j = 1$ . The points added to  $\mathcal{C}_-$  have neighborhoods homeomorphic to a neighborhood of a boundary point of  $H^9$ , the 9-dimensional half-space, so they are typical boundary points. Physically,  $|\vec{n}_0| = 1$  or  $|\vec{n}_1| = 1$  indicates a pure state of qubit  $A$  in one term of superposition.

2.  $p = 0$ . For any continuous extension of  $f$  to the points with  $p = 0$  we find that the new points for the generalized Bloch vector are given by

$$\begin{aligned} N_{0i} &= n_{1i} \\ N_{i0} &= -m_i \\ N_{ij} &= -m_i n_{1j}. \end{aligned}$$

Again, since the set of allowed  $N_{0i}$  and  $N_{ij}$  is independent of  $p$ , the only effect of varying  $p$  is to vary the magnitude of  $N_{i0}$ .  $p = 0$  corresponds to unit radius. Adding  $p = 0$  to the domain of  $f$  thus adds the boundary of  $B_3$  to the set of allowed  $N_{i0}$  and again these are typical boundary points of  $\mathcal{C}_-$ . Physically, this value of  $p$  corresponds to a product state: qubit  $B$ , in a mixed state for all  $p > 0$ , is now in a pure state given by  $\vec{m}$  and qubit  $A$  is in an arbitrary mixed state specified by  $\vec{n}_1$ . There is no correlation whatever between  $A$  and  $B$ .

3.  $p = 1/2$ . These points also lie in the closure of  $\mathcal{A}$ . Now we obtain an extension of  $f$  whose image includes the new points

$$N_{0i} = \frac{1}{2}(n_{0i} + n_{1i}) \quad (9)$$

$$N_{i0} = 0 \quad (10)$$

$$N_{ij} = \frac{1}{2}m_i(n_{0j} - n_{1j}). \quad (11)$$

We need only consider the change in the set of allowed  $N_{i0}$ , since the set of allowed  $N_{0i}$  and  $N_{ij}$  is not affected by  $p$ , as already noted. The only points of  $\mathbb{R}^{15}$  that are added to  $\text{im } f$  are those with  $N_{i0} = 0$  - otherwise there is no change. For any fixed  $p < 1/2$ ,  $\mathcal{C}_-$  restricted to the 3-dimensional subspace  $N_{0i}$  is an open 3-ball with the origin subtracted out. For  $p = 1/2$ , the image of any extension of  $f$  restricted to the 3-dimensional subspace  $N_{i0}$  is the origin, for which  $N_{0i}, N_{i0}$  and the  $N_{ij}$  all vanish. The origin is a 0-dimensional object, so any extension of  $f$  that includes  $p = 1/2$  in its domain will not be invertible. The origin does lie in  $\mathcal{C}$ , of course. However, it is easy to show that it is not a simple boundary point. All of the 15 coordinate axes belong to  $\mathcal{C}$  and they intersect at the origin. This implies that the origin does not have a neighborhood in  $\mathcal{C}$  that is homeomorphic to an open set of  $\mathbb{R}^9$ . Hence  $\mathcal{C}$  itself is not a manifold. Physically, at  $p = 1/2$  the qubit  $B$  is in the completely mixed state and any partial density matrix is possible for qubit  $A$ .

The addition of points in classes 1 and 2 do not affect the algebraic topology of  $\mathcal{C}_-$ . They are essentially boundary points and any path passing through these points can be deformed into a path that lies entirely in  $\mathcal{C}_-$ . This is probably also the case for points in class 3, which leads to the conjecture that  $\mathcal{C}$  itself is simply-connected. We do not have a proof of this, however.

To summarize, we find that  $\mathcal{C}_- \subset \mathcal{C}$  is a simply-connected 9-manifold without boundary. The homeomorphism  $f$  provides an embedding of  $\mathcal{C}_-$  into the 15-dimensional space  $\mathcal{M}$  of all density matrices, defining a 9-dimensional hypersurface that differs from  $\mathcal{C}$  itself by a set of measure zero.

Some additional properties of the hypersurfaces are:

(1)  $\mathcal{C}_-$  includes points infinitesimally close to the origin, (the point having  $N_{i0} = N_{0i} = N_{ij} = 0$ ).  $\mathcal{C}$  includes the origin itself.

(2)  $\mathcal{C}$  includes intervals lying on all 15 of the coordinate axes (points for which only one of the  $N_{i0}, N_{0i}, N_{ij}$  is nonzero). See appendix B for the proof. For example the  $N_{0x}$  axis corresponds to  $p = 1/2, n_{0x} = n_{1x} \neq 0, n_{0y} = n_{0z} = n_{1y} = n_{1z} = 0$ ; the  $N_{0x}$  axis corresponds to  $m_x = 1, m_y = m_z = 0, \vec{n}_0 = \vec{n}_1 = 0$ . The  $N_{xy}$  axis corresponds to  $p = 1/2, m_x = 1, m_y = m_z = 0, n_{0y} = -n_{1y} \neq 0$ , all others zero.

(3) The four eigenvalues of  $\rho_{AB} \in \mathcal{C}$  are:

$$\begin{aligned}\lambda_{1,2} &= \frac{1}{2}p \left(1 \pm |\vec{n}_0|^2\right) \\ \lambda_{3,4} &= \frac{1}{2}(1-p) \left(1 \pm |\vec{n}_1|^2\right).\end{aligned}$$

Pure states have one eigenvalue equal to one and the others zero, which means  $p = 0, |\vec{n}_0| = 1$  and  $\vec{n}_1 = 0$ . These points lie on  $\partial\mathcal{C}_-$ , the boundary of  $\mathcal{C}_-$ . The pure concordant states are just the usual pure product state and belong to a 4-manifold  $\mathcal{P}_\mathcal{C}$ . Expressed in terms of density matrices, any state of this type is classical-classical with a single product of projections operators, i.e. its density matrix is of the form  $\rho = |\Psi_a\rangle\langle\Psi_a| \otimes |\Psi_b\rangle\langle\Psi_b|$ .

In what follows, we will often refer to the set  $\mathcal{C}$  rather than  $\mathcal{C}_-$ , since many of our considerations do not depend on the fact that  $\mathcal{C}$  is not itself a manifold structure;  $\mathcal{C}$  and  $\mathcal{C}_-$  differ by only a set of measure zero.

## B. Parameterization of $\mathcal{C}$ (calculus on $\mathcal{C}$ )

We may calculate the 9 tangent vectors, namely  $\{\vec{t}_i = \partial f / \partial x_i\}$ ;  $i = 1$  to 9, where  $x_1 = \theta, x_2 = \phi$  are the spherical polar coordinates for  $\vec{m}$ ,  $x_3 = p, x_4 = n_{01}$ , etc. The explicit forms of the  $\vec{t}_i \in \mathbb{R}^{15}$  are in appendix D. We show there that these 9 tangent vectors form a linearly independent set almost everywhere in  $\mathcal{C}$ , i.e., that if there exists a set of real numbers  $\{c_1, c_2, c_3, \dots, c_9\}$  such that  $c_1 \vec{t}_1 + c_2 \vec{t}_2 + c_3 \vec{t}_3 + \dots + c_9 \vec{t}_9 = \vec{0}$  then  $c_1 = c_2 = \dots = c_9 = 0$ . This procedure fails when any of the  $\vec{t}_i$  vanish. This occurs at the purely coordinate singularities  $\theta = 0$  and  $\theta = \pi$ , which are not truly singular points. It also happens at points with  $p = 1/2, \vec{n}_0 = \vec{n}_1$  and at the points  $p = 0$ . As we have seen above, these correspond to real singular points. However, since they occupy a set of measure zero, the parametrization with  $\theta, \phi, p, \vec{n}_0, \vec{n}_1$  can be used for integration with the 9-surface element

$$dS = \sqrt{|g|} d\theta d\phi dp \dots dn_{11} dn_{12} dn_{13}$$

where  $g$  is the appropriate matrix tensor

$$g = (g_{ij}).$$

$g$  consists of elements  $g_{ij} = \vec{t}_i \cdot \vec{t}_j$ . Most of the off-diagonal elements of  $g$ 's are zero (see the full matrix form in appendix D). We obtain  $\sqrt{|g|} = 16p^3(1-p)^3 \sin\theta \{ \sum_{i=1}^3 [pm_{0i} - (1-p)n_{1i}]^2 + (1-2p)^2 \}$ .

## C. 2-dimensional and 3-dimensional cross sections of $\mathcal{C}$

It is difficult to visualize a 9-dimensional structure such as  $\mathcal{C}$ . Accordingly, we consider sections of  $\mathcal{C}$ : intersections of  $\mathcal{C}$  with coordinate planes obtained by setting some coordinates of  $\mathbb{R}^{15}$  equal to zero. In particular, we will consider 2-sections for which 13 coordinates are zero, and 3-sections for which 12 coordinates are zero. This will help to make clear the differences between entanglement and discord. Because of the fact that  $\mathcal{M}$  and  $\mathcal{S}$  are convex 15-dimensional sets that include the origin, the 2-sections of  $\mathcal{M}$  and  $\mathcal{S}$  are all 2-dimensional convex sets. In fact all 2-sections of  $\mathcal{M}$  are either squares or disks centered at the origin<sup>19</sup>. (Note that using a different basis, such as the Gell-Mann matrices<sup>29</sup>, can result in the presence of other types of geometry for the 2-sections such as triangles and parabolas.) Zhou *et al.*<sup>19</sup> were able to show that the occurrence of squares and disks is determined by the commutativity properties of the operators corresponding to the two axes: squares for commuting operators and disks for non-commuting operators. Since the shape of  $\mathcal{M}$  is determined by positivity conditions on the eigenvalues; this is not so surprising: the contribution of the coefficients  $N_{ij}$  add in quadrature to the eigenvalues of the non-commuting case.

Making a complete survey of the 2-sections of  $\mathcal{C}$  reveals interesting similarities and differences to those of  $\mathcal{M}$ , as shown in Tab. (I). There are three geometries observed for  $\mathcal{C}$ : the square, the disk, and the cross. The first two are the same as for  $\mathcal{M}$ , and presumably reflect similar physics, but the cross is new and it occupies about one third of the table. It is the union of the two line intervals  $[-1, 1]$  lying in the two Cartesian axes. This is a locally 1-dimensional object (except at the origin, where the intersection of the intervals occurs), which reflects the lower dimensionality of  $\mathcal{C}$ , as compared to  $\mathcal{S}$  or  $\mathcal{M}$ . Furthermore, unlike entangled states, there are discordant states arbitrarily close to the origin.

Using the explicit form for the 15 components of  $N$ 's for a concordant state as expressed in Eqs. (5) and (7), the disk and square of  $\mathcal{C}$  are always specified with 2 independent variables while this is not possible for the cross; the only two nonzero components of the intersecting plane of the state cannot be nonzero at the same time if we are to have zero discord.

An explicit example for the square is the state  $\rho = \frac{I}{4} + \frac{1}{4}N_{10}\sigma_1 \otimes \sigma_0 + \frac{1}{4}N_{13}\sigma_1 \otimes \sigma_3$ ,  $I$  is the identity matrix. This is a concordant subset of  $\mathcal{M}$  obtained when  $n_{02} = n_{03} = n_{12} = n_{13} = m_2 = m_3 = 0, m_1 = \pm 1$ , and  $n_{01}$  ( $= n_{11}$ ) and  $p$  are freely chosen from  $\mathcal{A}$  such that  $N_{10} = \pm(2p-1)$  and  $N_{13} = \pm 2pn_{01}$ .

For the cross geometry, consider the example  $\rho = \frac{I}{4} + \frac{1}{4}N_{10}\sigma_1 \otimes \sigma_0 + \frac{1}{4}N_{21}\sigma_2 \otimes \sigma_1$ . The states of this set are discordant everywhere except on the coordinate axes. The concordant states have only a single nonzero component, either of  $N_{10} = (2p-1)m_1$  and  $N_{21} = 2pm_2n_{01}$ . Specifically, in order for both  $N_{10}$  and  $N_{21}$  to be nonzero,

the product  $2(2p-1)m_1m_2pn_{01} \neq 0$ . But this implies that  $N_{11} = 2m_1pn_{01} \neq 0$ ,  $N_{20} = (2p-1)m_2 \neq 0$ .

Let us consider the positions of the cross geometry in more detail, since this geometry is unique to discord. States in a 2-section have the form

$$\rho = \frac{I}{4} + \frac{1}{4}N_{ij}\sigma_i \otimes \sigma_j + \frac{1}{4}N_{kl}\sigma_k \otimes \sigma_l$$

so that we can refer to the  $ij, kl$  section with  $0 \leq i, j, k, l \leq 3$ . We first note that crosses occur only when at least one correlation function is involved, i.e., at most one of the  $j, l$  can be zero. [This observation is related to the fact that we have considered the “left” discord measure, which is, in this case, on qubit A. Similar statements hold for  $i, k$  for the “right” discord measure.] This is expected, since discord requires correlation. An example of a density matrix with cross behavior is

$$\rho = \frac{I}{4} + \frac{1}{4}N_{10}\sigma_x \otimes \sigma_0 + \frac{1}{4}N_{21}\sigma_y \otimes \sigma_x.$$

When  $0 < |N_{10}| \ll 1$  and  $0 < |N_{21}| \ll 1$ , this state is separable but discordant. This emphasizes the fact that discord, as compared to entanglement, is much more resistant to dephasing, since states of this kind can be arbitrarily close to the origin where the system is completely dephased. This state contains quantum correlation because it combines the non-commuting operators  $\sigma_x\sigma_0$  and  $\sigma_y\sigma_x$ . The choice of how to measure qubit 1 (along the x-axis or along the y-axis) can have some effect on how much information we gain about qubit 2. Finally, we look at the case when all of the  $i, j, k, l$  are nonzero. Crosses occur if and only if  $i \neq k$  and  $j \neq l$ , e.g.,

$$\rho = \frac{I}{4} + \frac{1}{4}N_{11}\sigma_x \otimes \sigma_x + \frac{1}{4}N_{23}\sigma_y \otimes \sigma_z$$

with  $0 < |N_{11}| \ll 1$  and  $0 < |N_{23}| \ll 1$  is separable but discordant, but

$$\rho = \frac{I}{4} + \frac{1}{4}N_{11}\sigma_x \otimes \sigma_x + \frac{1}{4}N_{12}\sigma_x \otimes \sigma_y$$

with  $0 < |N_{11}| \ll 1$  and  $0 < |N_{12}| \ll 1$  (a disk state) is separable and concordant. It seems that since measuring qubit 1 along the y or z axes gives no non-trivial information, the choice involved does not generate discord.

An examination of the 3-sections of  $\mathcal{C}$  is also revealing. Such a state is of the form  $\rho = \frac{I}{4} + \frac{1}{4}N_{ij}\sigma_i \otimes \sigma_j + \frac{1}{4}N_{kl}\sigma_k \otimes \sigma_l + \frac{1}{4}N_{mn}\sigma_m \otimes \sigma_n$ . Since three nonzero coefficients are necessary to form a maximally entangled (pure) state, the 3-sections bring in qualitatively new physics. If the 3-section does include maximally entangled states, then these states occupy the vertices of a tetrahedron geometry, as shown previously for the Bell states<sup>21</sup>. We show that the 3-sections can have zero or nonzero 3-volume. Using this fact and the table of 2-section geometries [Tab. (I)] we can characterize all allowed 3-section geometries.

	1	2	3	4	5	6	7	8	9	10	11	12	13	14	15
OX	1														
OY	2	D													
OZ	3	D	D												
X0	4	S	S	S											
Y0	5	S	S	S	D										
Z0	6	S	S	S	D	D									
XX	7	S	D	D	S	+	+								
XY	8	D	S	D	S	+	+	D							
XZ	9	D	D	S	S	+	+	D	D						
YX	10	S	D	D	+	S	+	D	+	+					
YY	11	D	S	D	+	S	+	+	D	+	D				
YZ	12	D	D	S	+	S	+	+	+	D	D	D			
ZX	13	S	D	D	+	+	S	D	+	+	D	+	+		
ZY	14	D	S	D	+	+	S	+	D	+	+	D	+	D	
ZZ	15	D	D	S	+	+	S	+	+	D	+	+	D	D	D

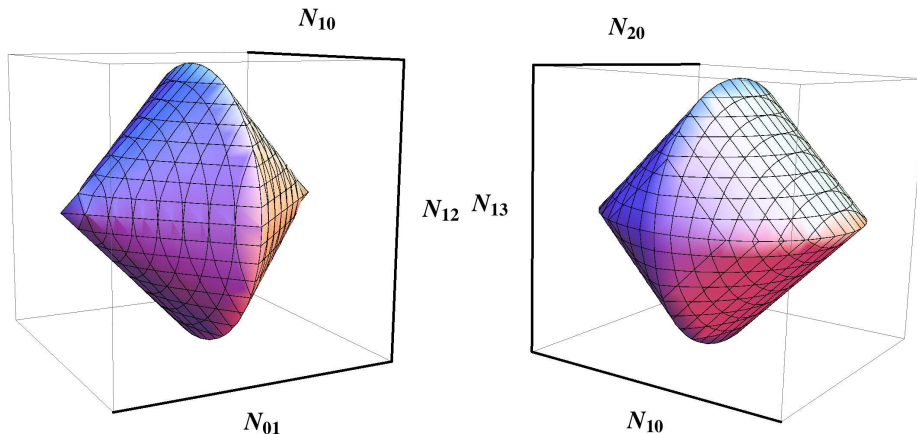
TABLE I: Possible geometries of the 2-sections of the concordant subset  $\mathcal{C}$ . D and S stand for disk and square, respectively. Crosses denote the union of two intervals on the two Cartesian axes.

When a 3-section has nonzero volume, it is specified by a set of three independent parameters drawn from  $\mathcal{A}$ . As a relatively simple example, consider the 3-section obtained by varying  $p, n_{01}$ , and  $n_{11}$ , setting  $m_2 = m_3 = n_{02} = n_{03} = n_{12} = n_{13} = 0$  and  $m_1 = 1$ . The 3 remaining parameters  $p, n_{01}$ , and  $n_{11}$  are arbitrary. Consider  $m_1 = 1$ . Then we find that the allowed values of  $N_{01} = pn_{01} + (1-p)n_{11}$ ,  $N_{10} = (2p-1)$ ,  $N_{11} = pn_{01} - (1-p)n_{11}$  form a tetrahedron. Note that  $N_{01}, N_{10}, N_{11}$  defined in this way are independent of one another: the subclass of states having the density matrix  $\rho = \frac{1}{4}(\sigma_0 \otimes \sigma_0 + N_{01}\sigma_0 \otimes \sigma_1 + N_{10}\sigma_1 \otimes \sigma_0 + N_{11}\sigma_1 \otimes \sigma_1)$  contains all physical states in a tetrahedron that is identical to the concordant tetrahedron specified before by the set of parameters  $\{p, n_{01}, n_{11}\}$ .

We now make the observation that the 2-sections of this tetrahedral 3-section obtained by intersection with the  $\{N_{01}, N_{10}\}$ ,  $\{N_{01}, N_{11}\}$  and  $\{N_{10}, N_{11}\}$  planes are all squares [see Tab. (I)]. This is in fact true of any combination of  $\{N_{0i}, N_{j0}, N_{ji}\}$  (9 combinations in total) that forms a tetrahedron of concordant states and leads to the classification of all nonzero-volume 3-sections into 4 types.

1. Tetrahedron when all 3 2-sections are squares.
2. Unit ball when all 3 2-sections are disks. For example, the combination  $\{N_{01}, N_{02}, N_{03}\}$  by setting  $p = 1/2$ ,  $\vec{n}_0 = \vec{n}_1$  is in this class. Now,  $N_{0i} = n_{0i}$  independent of  $\vec{m}$ . Similarly to the tetrahedron case discussed above, all three components are independent of one another, which indicates that any physical state made of three component  $N_{0i}$  is a concordant state. This property holds for other combinations such as  $\{N_{10}, N_{20}, N_{30}\}$  by setting  $\vec{n}_0 = \vec{n}_1 = 0$  or  $\{N_{11}, N_{12}, N_{13}\}$  by setting  $p = 1/2$ ,  $\vec{n}_0 = -\vec{n}_1$ , and  $m_2 = m_3 = 0$ , etc.
3. Union of 2 cones when 1 2-section is a square and 2 are disks. The object can be thought of as 2 cones

FIG. 4: Two possible 3-sections of the concordant set  $\mathcal{C}$  with nonzero 3-volume. On the left is a union of 2 cones (case 3 below), while on the right is a more complex, less easily characterized object (case 4 below)



glue together at their bases or as the surface of revolution formed when a square is rotated about an axis that passes through its center. See Fig. 4 (left).

4. A less easily described 3-dimensional object shown in Fig. 4 (right), when the 1 2-section is a disk and 2 2-sections are squares. For example, the combination  $\{N_{01}, N_{10}, N_{12}\}$  obtained by setting  $m_2 = m_3 = n_{03} = n_{13} = 0$  and  $pn_{01} = (1-p)n_{11}$  and  $pn_{02} = -(1-p)n_{12}$ . This 3-section has 2-sections are a set of 2 squares  $[\{N_{01}, N_{10}\}]$  and  $[\{N_{01}, N_{12}\}]$  and 1 disk  $[\{N_{10}, N_{12}\}]$ , etc.

Last, we consider 3-sections with zero 3-volume. Its 2-sections include at least one cross. Analytically, such a 3-section is specified by a union of sets of equations and each set has at most 2 independent variables. An example is the 3-section with nonzero  $\{N_{01}, N_{10}, N_{21}\}$  obtained by setting either 1)  $m_2 = m_3 = n_{02} = n_{03} = n_{12} = n_{13} = 0$  and  $pn_{01} = (1-p)n_{11}$  i.e. by at most 2 independent parameters  $(p, n_{01})$  or  $(p, n_{11})$  or 2)  $m_1 = m_3 = n_{02} = n_{03} = n_{12} = n_{13} = 0$  and  $p = 1/2$  i.e. by 2 independent parameters  $(n_{01}, n_{11})$ . If there are 3 crosses among the 2-sections, then the 3-section is locally 1-dimensional. The extreme example is the Bell-diagonal state with nonzero  $\{N_{11}, N_{22}, N_{33}\}$  that has a 3-section that is the union of 3 1-section objects - the coordinate axes.

#### IV. TIME EVOLUTION OF DISCORD

We now turn to the consequences of the topological analysis for the time evolution of the quantum discord in 2-qubit systems. We are mainly interested in decoherence, so we will assume that the initial state of the system has finite discord that decreases overall, though perhaps not monotonically, as time increases. The opposite behavior is obviously possible: take a 2-qubit system in the fully mixed state and let it relax to an entangled ground state by reason of contact with a cold bath.

Hence we consider functions  $D_G(\vec{N}(t))$ , where  $\vec{N}$  is

the 15-dimensional real generalized Bloch vector and  $D_G$  is the geometric discord. We will further assume that the system tends to a limit as the time approaches infinity:  $\lim_{t \rightarrow \infty} \vec{N}(t) = \vec{N}_\infty$  and  $D_{G\infty} = D_G(\vec{N}_\infty)$ . If there are no self-intersections, the trajectory  $\{\vec{N}(t) | 0 \leq t < \infty\}$  itself is a 1-dimensional manifold.

We briefly review the analysis of evolution entanglement. For any evolution, we define the set of times when the entanglement vanishes:  $T_0^S = \{t | C(\vec{N}(t)) = 0\}$ , where  $C$  is the concurrence<sup>32,33</sup>. In previous work<sup>20</sup>, transversality theory was applied to the intersections of trajectories with the set  $\mathcal{S}$  to analyze the possible forms of  $T_0^S$ . It was found that when the trajectory and  $\mathcal{S}$  are transversal, (the generic case), then entering behavior, E, [entanglement sudden death,  $T_0^S = (t_c, \infty)$ ] or oscillating, O, ( $T_0^S$  a union of finite intervals) are the first two possible behaviors of the entanglement. It follows from transversality theorems that they are both stable under small perturbations. The other two behaviors occur when transversality is violated, which requires a symmetry in the dynamics or other special conditions - then we can get half-life (approaching), A, behavior ( $T_0^S = \emptyset$ ) or bouncing, B, behavior, when  $T_0^S$  is a collection of isolated points. These two latter behaviors are unstable to small perturbations.

The condition for transversality theorems to hold is that the sum of the dimensions of the intersecting manifolds be at least as great as the dimension of the underlying space, which holds for trajectories (which have dimension 1) and  $\mathcal{S}$  since  $\dim \mathcal{S} + 1 = 16 > 15 = \dim M$ . Since  $\dim \mathcal{C} = 9 < 14 = \dim M - 1$ , we cannot use the same reasoning for discord evolution. Let us define  $T_0^D = \{t | D_G(\vec{N}(t)) = 0\}$ . If we assume that  $\vec{N}(t)$  has a continuous first derivative and that  $D_{G\infty} = 0$ , there are two possibilities: ( $T_0^D = \emptyset$ , the null set) (“half-life”) or  $T_0^D$  is a collection of isolated points (bouncing behavior), and neither of these categories is stable with respect to

small perturbations. They happen only as a result of particular choices, when the discord has a non-trivial relationship to the dynamics. This can happen naturally - for example, the origin  $\vec{N} = 0$  belongs to  $C$  and  $\vec{N}_\infty = 0$  for a system in contact with a bath at high temperature.

### A. Unitary Evolution

#### Introduction

Having classified the various possibilities for the evolution of entanglement and discord, we now turn to the question of the realization of these evolutions in explicit models. In this regard, it is useful to distinguish between unitary evolution of the density matrix and non-unitary evolutions. This distinction is of course crucial for the experimental investigation of all types of coherence: unitary time evolution is by definition coherent overall, all correlation measures should be unchanged by local unitary evolution, but the behavior of different correlation measures under nonlocal unitary time evolution can help to understand the distinctions between different measures.

#### Ising model

The Ising Hamiltonian:

$$H^I = J\sigma_3 \otimes \sigma_3 \quad (12)$$

generates a two-qubit unitary operator of the system of the form:

$$\begin{aligned} U &= \exp(-iJt \sigma_3 \otimes \sigma_3) \\ &= \begin{pmatrix} e^{-iJt} & 0 & 0 & 0 \\ 0 & e^{iJt} & 0 & 0 \\ 0 & 0 & e^{iJt} & 0 \\ 0 & 0 & 0 & e^{-iJt} \end{pmatrix} \\ &= C \sigma_0 \otimes \sigma_0 - i S \sigma_3 \otimes \sigma_3 \end{aligned} \quad (13)$$

where we use the abbreviations  $S = \sin(Jt)$  and  $C = \cos(Jt)$ . This would be an appropriate Hamiltonian for well-separated superconducting flux qubits with the rings lying in the same plane when the applied field is zero.

Under the unitary transformation (13), any initial state of general form (2) evolves as:

$$\begin{aligned} \rho(t) &= \frac{1}{4}(\sigma_0 \otimes \sigma_0 + N_{0i}(t)\sigma_0 \otimes \sigma_i \\ &\quad + N_{i0}(t)\sigma_i \otimes \sigma_0 + N_{ij}(t)\sigma_i \otimes \sigma_j). \end{aligned} \quad (14)$$

There are 7 constants of motion:  $N_{03}, N_{30}, N_{33}, N_{12}, N_{21}, N_{11}, N_{22}$ . With these constraints, any system that is initialized in an  $\mathbf{X}$ -state has constant quantum discord in this model. This relatively simple model appears to be the most non-trivial model that has trivial dynamics for the discord for a reasonable wide class of states:  $D$  is completely independent of time for the 8-dimensional space of  $\mathbf{X}$ -states.

#### Heisenberg Model

A Heisenberg model with the presence of all XYZ terms i.e.  $H^H = J \sum_{i=X,Y,Z} \sigma_i \otimes \sigma_i$  is appropriate for electron spin qubits with overlapping wavefunctions, which will then feel the exchange interaction. The unitary transformation generated by  $H^H$  is of course much richer. The class of states with constant discord is the 3-dimensional space of Bell-diagonal states.

The remaining 8 components evolve under the unitary transformation (13) as:

$$\begin{aligned} N_{01}(t) &= N_{01}C_3 + N_{32}S_3 \\ N_{32}(t) &= N_{32}C_3 - N_{01}S_3 \\ N_{02}(t) &= N_{02}C_3 - N_{31}S_3 \\ N_{31}(t) &= N_{31}C_3 + N_{02}S_3 \end{aligned} \quad (15)$$

$$\begin{aligned} N_{10}(t) &= N_{10}C_3 + N_{23}S_3 \\ N_{23}(t) &= N_{23}C_3 - N_{10}S_3 \\ N_{20}(t) &= N_{20}C_3 - N_{13}S_3 \\ N_{13}(t) &= N_{13}C_3 + N_{20}S_3 \end{aligned} \quad (16)$$

where  $S_3 = \sin(2Jt)$  and  $C_3 = \cos(2Jt)$ .

Note that under a unitary transition the purity of the state is conserved i.e.  $|\vec{N}(t)|^2 = |\vec{N}|^2$ . The two separate groups with time dependent components of  $\rho(t)$  in Eqs. (15) and (16) are two groups of DQC1 separable states.

For purposes of illustration we choose the initial condition such that only  $N_{20}$  is nonzero and  $N_{20} = 1$  (a concordant state). The system evolves as:

$$\begin{aligned} N_{20}(t) &= C_3 \\ N_{13}(t) &= S_3 \end{aligned} \quad (17)$$

and is a separable state i.e.  $C(t) = 0$  with concordant subset as the union of  $N_{20}(t)$  and  $N_{13}(t)$  axes (see Tab. I). Quantum trajectory of the system is the unit circle  $N_{20}(t)^2 + N_{13}(t)^2 = 1$ .

The quantum discord of (17) is (see detailed calculations in Appendix E):

$$\begin{aligned} D(t) &= -\frac{1}{2}[(1 + C_3) \log(1 + C_3) + (1 - C_3) \log(1 - C_3)] \\ &\quad + 1 - \frac{1}{2}[(1 - S_3) \log(1 - S_3) + (1 + S_3) \log(1 + S_3)] \end{aligned}$$

and the geometric quantum discord is:

$$D_G(t) = \frac{1}{4}(1 - \max\{C_3^2, S_3^2\})$$

which are shown in Fig. 5. The entanglement is identically zero, while the discord oscillates with maximum ( $\approx 0.2$ ) at  $t = \frac{\pi}{16} + n\frac{\pi}{8}$  and vanishes at  $t = n\frac{\pi}{8}$ . In the semiclassical picture, the two spins precess about one another. We have chosen a starting state that is separable, and the mutual precession does not generate entanglement. This is true for nearly all separable initial conditions, so our choice of initial state is fairly generic. For

the discord, however, the situation is quite different. To have zero discord, the classical states of one subsystem need to pair up with the mixed states of the other. This requires additional phase relations. Because these phase relations are oscillating, we get a periodic behavior of the discord. Note that the geometric and quantum discord behave very similarly, as is nearly always the case. The only significant distinction is the linear (quadratic) zeros for the quantum (geometric) discord corresponding to the

linear and quadratic distance measures in the definitions.

### Anisotropic XY-model

Consider an anisotropic exchange Hamiltonian with cross-product terms:

$$H^{XY} = J_{xy}\sigma_x \otimes \sigma_y + J_{yx}\sigma_y \otimes \sigma_x. \quad (18)$$

The corresponding unitary operator is:

$$\begin{aligned} U(t) &= e^{-it(J_{xy}\sigma_x \otimes \sigma_y + J_{yx}\sigma_y \otimes \sigma_x)} \\ &= \begin{pmatrix} \cos(J_{xy} + J_{yx})t & 0 & 0 & -\sin(J_{xy} + J_{yx})t \\ 0 & \cos(J_{xy} - J_{yx})t & \sin(J_{xy} - J_{yx})t & 0 \\ 0 & -\sin(J_{xy} - J_{yx})t & \cos(J_{xy} - J_{yx})t & 0 \\ \sin(J_{xy} + J_{yx})t & 0 & 0 & \cos(J_{xy} + J_{yx})t \end{pmatrix} \\ &= C_1 C_2 \sigma_0 \otimes \sigma_0 - S_1 S_2 \sigma_3 \otimes \sigma_3 - i(S_1 C_2 \sigma_1 \otimes \sigma_2 + S_2 C_1 \sigma_2 \otimes \sigma_1) \end{aligned} \quad (19)$$

where  $S_1 = \sin(J_{xy}t)$ ,  $C_1 = \cos(J_{xy}t)$  and  $S_2 = \sin(J_{yx}t)$ ,  $C_2 = \cos(J_{yx}t)$ . These cross-product terms reflect the fact that the number of constants of motion decreases as compared to that of the Ising model and we expect to see different evolution behaviors for the quantum correlations in the Bell-diagonal class. Let us consider the situation where  $J_{xy} = -J_{yx}$ . The unitary operator simplifies

This model can arise from the Dzyaloshinskii-Moriya interaction between two electron spins whose separation vector is along the z-axis. Consider the initial state of the general form in Eq. (2). The state at time  $t$  is given by:

$$\begin{aligned} U(t) &= C_2^2 \sigma_0 \otimes \sigma_0 + S_2^2 \sigma_3 \otimes \sigma_3 \\ &\quad + i S_2 C_2 (\sigma_1 \otimes \sigma_2 - \sigma_2 \otimes \sigma_1). \end{aligned} \quad (20)$$

$$\begin{aligned} N_{03}(t) &= \frac{1}{2}[N_{03} + N_{30} + (N_{03} - N_{30}) \cos 4J_{yx}t + (N_{11} + N_{22}) \sin 4J_{yx}t] \\ N_{30}(t) &= \frac{1}{2}[N_{03} + N_{30} + (-N_{03} + N_{30}) \cos 4J_{yx}t - (N_{11} + N_{22}) \sin 4J_{yx}t] \\ N_{11}(t) &= \frac{1}{2}[N_{11} - N_{22} + (-N_{03} + N_{30}) \sin 4J_{yx}t + (N_{11} + N_{22}) \cos 4J_{yx}t] \\ N_{22}(t) &= \frac{1}{2}[-N_{11} + N_{22} + (-N_{03} + N_{30}) \sin 4J_{yx}t + (N_{11} + N_{22}) \cos 4J_{yx}t] \end{aligned} \quad (21)$$

and

$$\begin{aligned} N_{33}(t) &= N_{33} \\ N_{12}(t) &= N_{12} \\ N_{21}(t) &= N_{21} \end{aligned} \quad (22)$$

and

$$\begin{aligned} N_{01}(t) &= N_{01} \cos 2J_{yx}t - N_{13} \sin 2J_{yx}t \\ N_{13}(t) &= N_{01} \sin 2J_{yx}t + N_{13} \cos 2J_{yx}t \end{aligned} \quad (23)$$

$$\begin{aligned} N_{02}(t) &= N_{02} \cos 2J_{yx}t - N_{23} \sin 2J_{yx}t \\ N_{23}(t) &= N_{02} \sin 2J_{yx}t + N_{23} \cos 2J_{yx}t \end{aligned} \quad (24)$$

$$\begin{aligned} N_{10}(t) &= N_{10} \cos 2J_{yx}t + N_{31} \sin 2J_{yx}t \\ N_{31}(t) &= -N_{10} \sin 2J_{yx}t + N_{31} \cos 2J_{yx}t \end{aligned} \quad (25)$$

$$\begin{aligned} N_{20}(t) &= N_{20} \cos 2J_{yx}t + N_{32} \sin 2J_{yx}t \\ N_{32}(t) &= -N_{20} \sin 2J_{yx}t + N_{32} \cos 2J_{yx}t. \end{aligned} \quad (26)$$

In this XY-model, the discord of the Bell-diagonal class

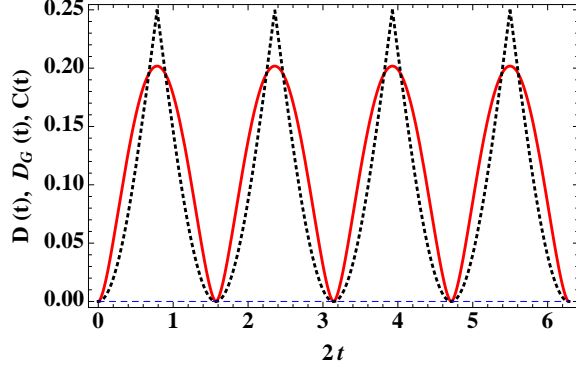


FIG. 5: (Color online) Time dependence of the quantum discord (red solid line), geometric discord (black dotted line), and concurrence (blue dashed line) of system described by (17).

of states is no longer independent of time. In the **X**-type of class of states, only the states with only three nonzero components  $\{N_{12}(t), N_{21}(t), N_{33}(t)\}$  have time-independent discord. All physical states of this type lie in the tetrahedron similar to the geometry of the Bell-diagonal states with the concordant subset as the union of the three intervals in the Cartesian axes.

A Werner state<sup>34</sup>:

$$\begin{aligned} \rho(0) = \rho_W(0) &\equiv \frac{1}{4}[\sigma_0 \otimes \sigma_0 - \alpha \sum_i \sigma_i \otimes \sigma_i] \\ &= \frac{1-\alpha}{4}I + \alpha|\Psi^-\rangle\langle\Psi^-| \end{aligned} \quad (27)$$

where  $|\Psi^-\rangle = \frac{|01\rangle - |10\rangle}{\sqrt{2}}$  and  $0 \leq \alpha \leq 1$  can exhibit sudden death/birth and oscillating behavior unitarily in this model. It evolves as:

$$\begin{aligned} N_{03}(t) &= -N_{30}(t) = -\alpha \sin 4J_{yx}t \\ N_{11}(t) &= N_{22}(t) = -\alpha \cos 4J_{yx}t \\ N_{33}(t) &= -\alpha. \end{aligned} \quad (28)$$

With the introduction of the mixing parameter  $\alpha$  we can also find transitions between different evolution categories.  $\alpha = 1$  is a pure maximally entangled state, while  $\alpha = 0$  is the completely mixed state. This Werner state is separable when  $\alpha \leq \frac{1}{3}$  (Eq. 27). As  $\alpha$  is varied, we find in the Bloch vector representation that  $(N_{11}, N_{22}, N_{33}) = (-\alpha, -\alpha, -\alpha)$ , so the vector lies on a line segment whose end points are the origin  $\alpha = 0$  and a point on the boundary of  $\mathcal{M}$ .

If the initial condition is  $\alpha = 1$ , the system evolves away from a maximally entangled situation. The concurrence and quantum discord are  $C(t) = |\cos 4J_{yx}t|$  and

$$\begin{aligned} D(t) &= 1 - \frac{1}{2}\{(\cos 2J_{yx}t + \sin 2J_{yx}t)^2 \log[(\cos 2J_{yx}t + \sin 2J_{yx}t)^2] \\ &\quad + (\cos 2J_{yx}t - \sin 2J_{yx}t)^2 \log[(\cos 2J_{yx}t - \sin 2J_{yx}t)^2]\}. \end{aligned} \quad (29)$$

The peaks of  $D(t)$  correspond to the two pure-state points of the 2 maximally entangled Bell states:  $N_{11}[t = (2n+1)\frac{\pi}{4}] = N_{22}(t) = -N_{33} = 1$  and  $N_{11}[t = (2n)\frac{\pi}{4}] = N_{22}(t) = N_{33} = -1$  while the vanishing discord points are two of the 4 pure-state points of the concordant tetrahedron  $\{N_{30}, N_{03}, N_{33}\}$  (see Fig. 6). Since the entanglement and the discord vanish at discrete points, this is **BB** joint evolution of entanglement and discord. When the initial condition is  $\alpha = 1/2$ , then the state starts as partially entangled. Evolution under the XY-Hamiltonian leads to entanglement death [ $C = 0$  in the region  $\frac{\pi}{12} + n\frac{\pi}{4} \leq t \leq \frac{\pi}{6} + n\frac{\pi}{4}$ ] and rebirth as illustrated in Fig. 6

$C$  can be computed explicitly as  $C(t) = \max\{0, \Delta_\lambda\}$  with  $\Delta_\lambda = \frac{1}{8}[\sqrt{9 + 4\cos 8J_{yx}t + 2\Delta} - \sqrt{9 + 4\cos 8J_{yx}t - 2\Delta} - 2]$  and  $\Delta = \sqrt{2\cos 16J_{yx}t + 18\cos 8J_{yx}t + 16}$ . This is **O**-type behavior.

The quantum discord in this case is:

$$\begin{aligned} D(t) &= \frac{5}{8} \log 5 - \frac{3 - 2 \sin 4J_{yx}t}{8} \log(3 - 2 \sin 4J_{yx}t) \\ &\quad - \frac{3 + 2 \sin 4J_{yx}t}{8} \log(3 + 2 \sin 4J_{yx}t). \end{aligned} \quad (30)$$

$D(t)$  vanishes at the discrete points  $t = \frac{\pi}{8} + n\frac{\pi}{4}$  as shown in Fig. 6(b). This is **B**-type behavior. These concordant points belong to the interior of the above tetrahedron. Thus the joint entanglement-discord evolution is of type **OB**.

This Werner class of states belongs to a more general class: the Bell-diagonal type:

$$\rho(0) = \rho_{\text{Bell}}(0) \equiv \frac{1}{4}[\sigma_0 \otimes \sigma_0 + \sum_i (N_{ii} \sigma_i \otimes \sigma_i)],$$

with arbitrary values for  $N_{11}, N_{22}$ , and  $N_{33}$ , each within the range  $[-1, 1]$ . In this larger class we find other types of joint evolution. For example, consider the initial state as the Bell-diagonal subclass with constraint

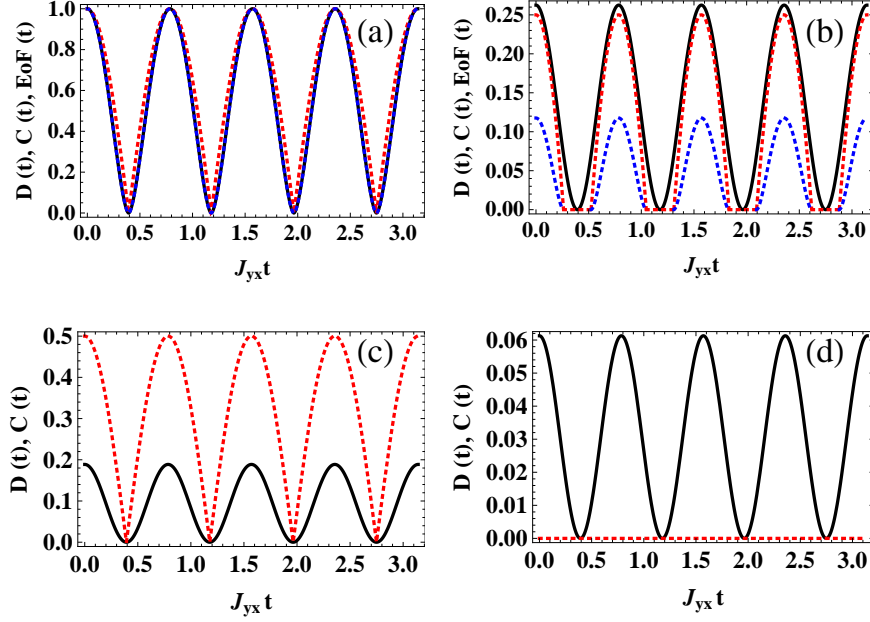


FIG. 6: (Color online) Time dependence of the quantum discord (black solid lines), concurrence (red dotted lines), and entanglement (blue dashed lines). For (a) and (b) the initial state is a Werner state with initial conditions  $\alpha = 1$  (a) and  $\alpha = 1/2$  (b), as defined in Eq. (27). The time evolution is given by Eq. (28). For (c) and (d) the initial state is a Bell-diagonal state that evolves according to Eq. (31) with entanglement parameter  $\beta = 1/2$  (c) and  $\beta = 1/4$  (d).

$N_{11} = N_{22} = -\frac{N_{33}}{2} = \beta$  with  $0 \leq \beta \leq 1/2$ . The time dependent Bloch vector becomes:

$$\begin{aligned} N_{03}(t) &= -N_{30}(t) = \beta \sin 4J_{yx}t \\ N_{11}(t) &= N_{22}(t) = \beta \cos 4J_{yx}t \\ N_{33}(t) &= N_{33}. \end{aligned} \quad (31)$$

The initial concurrence of this Bell-diagonal state is  $C(0) = \max\{0, (4\beta - 1)/2\}$  which implies that it is partially entangled for  $1/4 < \beta \leq 1/2$ . The concurrence evolves as:  $C(t) = \max\{0, \Delta_B\}$  where

$$\begin{aligned} \Delta_B &= \frac{1}{4} [\sqrt{1 + 4\beta + 8\beta^2 \cos 4J_{yx}t^2 + 4\beta \Gamma_B} \\ &\quad - \sqrt{1 + 4\beta + 8\beta^2 \cos 4J_{yx}t^2 - 4\beta \Gamma_B} \\ &\quad - 2(1 - 2\beta)] \end{aligned}$$

with  $\Gamma_B = \sqrt{\cos(4J_{yx}t)^2 (1 + 4\beta + 4\beta^2 \cos(4J_{yx}t)^2)}$ ; while the quantum discord in this case is given by:

$$\begin{aligned} D(t) &= \frac{5}{8} \log 5 - \frac{3 - 2 \sin 4J_{yx}t}{8} \log(3 - 2 \sin 4J_{yx}t) \\ &\quad - \frac{3 + 2 \sin 4J_{yx}t}{8} \log(3 + 2 \sin 4J_{yx}t). \end{aligned} \quad (32)$$

$D(t)$  vanishes at the discrete points  $t = \frac{\pi}{8} + n\frac{\pi}{4}$  as shown in Fig. 6(b). For  $\beta = 1/2$  the concurrence reduces to a simpler form  $C(t) = \frac{|\cos 4J_{yx}t|}{2}$  and the quantum discord

and quantum entanglement evolve in a relatively similar manner (bouncing) so that the joint evolution is again  $BB$  as seen in Fig. 6(c). The Bloch vector has the time dependent form given in Eq. (31). When  $\beta = 1/4$  we again have zero entanglement coexisting with oscillating discord as seen in Fig. 6(d)

## B. Non-unitary evolution

### Ising model with random telegraph noise

Now we study how the system decoheres using a minimal random telegraph noise model: an unbiased single-fluctuator random telegraph noise, in a Markovian or/and non-Markovian process subject to an applied magnetic field along the  $z$ -direction. Such a system can be described by the following Hamiltonian:

$$H = H^I + H^{RTN} + H^Z \quad (33)$$

where  $H^I = J \sigma_z \otimes \sigma_z$ ,  $H^{RTN} = s(t) g_z \sigma_z \otimes \sigma_0$ , and the Zeeman energy  $H^Z = B_z \sigma_0 \otimes \sigma_z$ .

Using the quasi-Hamiltonian method (cf. Refs.<sup>35,36</sup>) this problem can be solved exactly.

$$\vec{N}(t) = \langle f | e^{-iH_q t} | i \rangle \vec{N}_0$$

where  $|f\rangle \equiv |i\rangle = (1, 1)^T / \sqrt{2}$  and

$$H_q = i \lim_{\Delta t \rightarrow 0} \frac{\Gamma - \mathbf{I}_{30}}{\Delta t}$$

where

$$\Gamma = \begin{pmatrix} (1 - \gamma\Delta t)\mathbf{T}_0 & \gamma\Delta t\mathbf{T}_0 \\ \gamma\Delta t\mathbf{T}_1 & (1 - \gamma\Delta t)\mathbf{T}_1 \end{pmatrix}$$

and  $\mathbf{T}_0 = e^{-i\Delta t H[s(t)=1]}$  and  $\mathbf{T}_1 = e^{-i\Delta t H[s(t)=-1]}$  correspond to the temporal transfer matrix when the noise sequence switches from  $s = 1$  to  $s = -1$ , respectively, with transition rate  $\gamma$ .  $H_q$  is called the time-independent quasi-Hamiltonian<sup>36</sup>. Eigenvalues of  $H_q$  can contain imaginary numbers which give decay rates. Real parts of its eigenvalues appear in the oscillation frequencies. Note that all the three terms in (33) are mutually commuting so that the solution for the entire system can be obtained by solving each single-term Hamiltonian separately (see Appendix I). Above we obtained full closed forms for all Bloch vector components of the Ising model as the system evolves unitarily where the **X**-type class has all 7 components as constants of motion. This means that all these components are affected only by the noise and applied field parts of  $H$ . As a consequence, all states of **X**-type exhibit only categories **A** (for discord) and **A** and **E** (for entanglement) in Markovian regime. If the initial state is outside the **X**-type [union of the two subclasses (15) and (16)], its evolution type depends on  $J$ . For example, Eq. (17) now becomes

$$\begin{aligned} N_{20}(t) &= e^{-\gamma t} \cos(2Jt) F(R_0) \\ N_{13}(t) &= e^{-\gamma t} \sin(2Jt) F(R_0) \end{aligned} \quad (34)$$

where  $R_0 = \sqrt{g_z^2 - \gamma^2/4}$  and

$$F(R_0) = \frac{2R_0 \cosh(2iR_0t) - i\gamma \sinh(2iR_0t)}{(2R_0)}. \quad (35)$$

Note that these components are independent of the applied field  $B$ . The dynamical process is Markovian if  $\gamma/2 > g_z$  and non-Markovian if  $\gamma/2 < g_z$ . The quantum discord [analytic form obtained in Appendix F] of this system exhibits only category **B** and entanglement is 0 for all  $t$ .

The time evolution of the Bloch vector of the Bell-diagonal state in this model is:

$$\begin{aligned} N_{11}(t) &= N_{11} e^{-\gamma t} F(R_0) \cos(2B_z t) \\ N_{12}(t) &= -N_{11} e^{-\gamma t} F(R_0) \sin(2B_z t) \\ N_{21}(t) &= N_{22} e^{-\gamma t} F(R_0) \sin(2B_z t) \\ N_{22}(t) &= N_{22} e^{-\gamma t} F(R_0) \cos(2B_z t) \\ N_{33}(t) &= N_{33}. \end{aligned} \quad (36)$$

This model yields a wide range of possible joint evolutions depending on initial conditions. For the Werner state with  $\alpha = 1/4$ , we get zero entanglement at all times, and the discord shows **A** behavior, as shown in Fig. 7(a). For  $\alpha = 1/2$ , we find **E**-type (sudden death) behavior, while the discord shows **A** behavior. For  $\alpha = 1$ , we find **A**-type behavior for both types of correlation. These evolutions are all in the Markovian regime. We illustrate two categories **A** and **E** for quantum correlations in Figs. 7(a)

- (c) for the Werner state (27) in a Markovian regime. Discord at time  $t$  of this state is obtained in Appendix G. In case  $\alpha = 1$ :

$$\mathcal{D}(t) = 1 + \lambda_+ \log \lambda_+ + \lambda_- \log \lambda_-$$

where  $\lambda_{\pm} = \frac{1 \pm \sqrt{N_{11}(t)^2 + N_{12}(t)^2}}{2}$  and the corresponding concurrence is:

$$\begin{aligned} 2C(t) &= |N_{11}(t)| + \sqrt{1 - N_{12}(t)^2} - ||N_{11}(t)| \\ &\quad - \sqrt{1 - N_{12}(t)^2}|. \end{aligned} \quad (37)$$

### XY-model with random telegraph noise

$$H = H^{XY} + H^{RTN} + H^Z$$

where  $H^{XY} = J_{xy}(\sigma_x \otimes \sigma_y - \sigma_y \otimes \sigma_x)$ . This is more complicated than the Ising case (see Appendix H) as the XY-term does not commute with the noise and the B-field terms. Consider the initial state as Werner state (27). The Bloch vector of the system evolves as:

$$\begin{aligned} N_{03}(t) &= -N_{30}(t) \\ N_{12}(t) &= -N_{21}(t) \\ N_{11}(t) &= N_{22}(t) \\ N_{33}(t) &= N_{33} (= -\alpha). \end{aligned} \quad (38)$$

$N_{12}(t)$  and  $N_{21}(t)$  are addition elements when noise is added as compared to the case without noise (see the corresponding unitary transformation).

In the evolutions generated by the XY-Hamiltonian, oscillations occur in the two correlation measures, and we find zero entanglement and **B** behavior for the discord for  $\alpha = 1/4$ , while  $\alpha = 1/2$  leads to **BB** behavior for the joint evolution, and  $\alpha = 1$  gives **OB** joint evolution, with the behavior of the entanglement given first. The actual evolutions are shown in Figs. 7(d), (e), (f).

Note that the quantum discord never quite vanishes for this case of the applied field on the second qubit  $B_z$  which guarantee two components  $N_{12}(t) = -N_{21}(t) \neq 0$  (which are zero in the case of the unitary transformation). Recall that for the unitary evolution, the quantum discord vanishes at  $\frac{\pi}{12} + n\frac{\pi}{4} \leq J_{yx}t \leq \frac{\pi}{6} + n\frac{\pi}{4}$  when  $N_{11}(t) [= N_{22}(t)]$  is zero. At that point, the Bloch vector  $\vec{N}(t) = \{N_{03}(t), N_{30}(t), N_{33}(t)\}$  and this state lies in one of the concordant subsets.

In both Markovian and non-Markovian regimes the interaction between the qubits is kept the leading contribution to the total energy of the entire system. As the noise strength is increased compatible to the interaction term the discord decays much rapidly. We note some quantitative differences in the Markovian and non-Markovian evolutions, but the evolution categories do not change, since the origin of the categories is topological.

### Noise effect comparison on Ising- and XY-models.

We note that the noise affects the quantum discord evolution in case of the Ising model stronger than that in

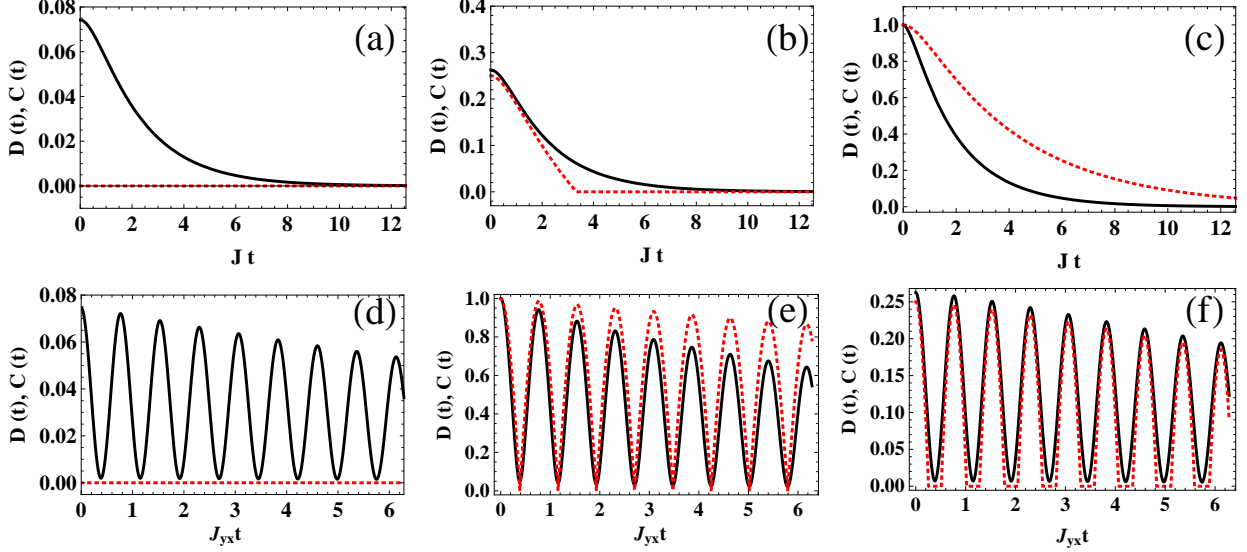


FIG. 7: (Color online) Six possible categories for the joint evolution of quantum discord (solid lines) and entanglement (dashed lines). The initial state is the Werner state defined in Eq. (27) [with  $\alpha = 1/4$  for (a) and (d),  $\alpha = 1/2$  for (b) and (e), and  $\alpha = 1$  for (c) and (f)]. The Markovian evolution is characterized by the parameters  $\gamma = J = J_{yx} = 3g_z = 3B_z = 1$ . Top panels are results obtained using the Ising Hamiltonian and bottom panels are from the XY-model.

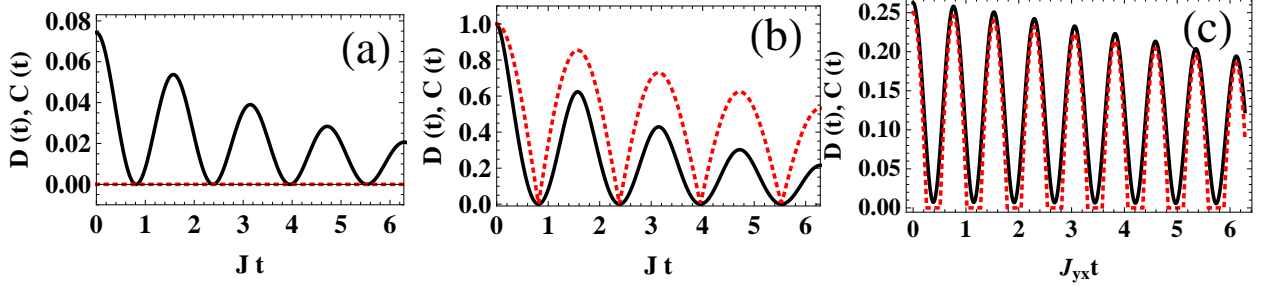


FIG. 8: (Color online) Three categories (seen in both Ising and XY-models) for the joint evolution of quantum discord (solid lines) and entanglement (dashed lines). The initial state is the Werner state defined in Eq. (27) with  $\alpha = 1/4$  for (a),  $\alpha = 1$  for (b), and  $\alpha = 1/2$  for (c). The evolution is non-Markovian and is characterized by the parameters  $\gamma = 0.27, J = J_{yx} = 3g_z = 3B_z = 1$ . (a) and (b) are obtained using the Ising model and (c) the XY-model.

case of the anisotropic exchange Hamiltonian (the  $H^{XY}$  model). As  $g_z$  is increased the discord vanishes faster than that in the case of the  $H^{XY}$  model.

**Noise correlation effect** We obtain the closed forms of the time dependence of all Bloch vector components in case the qubits interact with each other through the Ising spin exchange and with the two separate uncorrelated RTN sources of different transition rates  $\gamma_1 = \gamma, \gamma_2 = \xi\gamma$  ( $\xi > 0$ ). Full analytical solution for a general state can be obtained in Appendix I. As shown in Appendix I the RTN noise on qubit 1 does not affect subclass (15), the RTN noise on qubit 2 does not affect subclass (16), and the mutual qubit interaction does not affect the  $\mathbf{X}$ -type class [see Eq. (13)]. This phenomenon is understood using decoherence-free subspace theorem<sup>37</sup>. For  $J = 0$ ,

all components in each of the three separate above subclasses have similar time-dependent part and only differ by their initial condition  $N_{ij}(t=0)$ . Enhancement of the noise effect is seen in the  $\mathbf{X}$ -type of class: e.g. for  $\xi = 1$  a Bell-diagonal state at time  $t$  has:

$$\begin{aligned} N_{ii}(t) &= N_{ii} e^{-2\gamma t} G(R_0); \quad i = 1, 2 \\ N_{33}(t) &= N_{33} \end{aligned} \quad (39)$$

where

$$\begin{aligned} G(R_0) &= \frac{1}{8R_0^2} [4g_z^2 + (4R_0^2 - \gamma^2) \cosh(4iR_0t) \\ &\quad - 4i\gamma R_0 \sinh(4iR_0t)]. \end{aligned} \quad (40)$$

Fig. 9(a) shows the decoherence characteristic using this model for a system initially prepared in a partially en-

tangled Werner state (27) for  $\alpha = 0.8$ . The quantum entanglement exhibits category O i.e. the entanglement will repeatedly disappear within some certain time period while the discord only disappears at discrete time points.

The bottom sketch describes another non-Markovian process for the correlated noise case where the trajectory never visits the origin and only approaches this point as  $t \rightarrow \infty$ . Both quantum entanglement and discord never quite vanish in the B-like category.

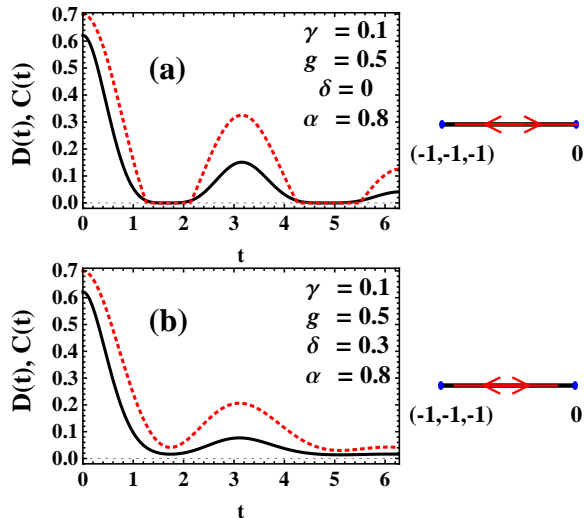


FIG. 9: (Color online) Joint evolution of discord (solid lines) and entanglement (dashed lines) of a system subject to uncorrelated (a) and correlated (b) telegraph noise. The switching rate  $\gamma$  is the same for the (a) and (b). The dynamics are non-Markovian with Ising interaction and the initial state is a Werner state with  $N_{xx} = N_{yy} = N_{zz} = -\alpha = 0.8$ . The sketches on the right-hand-side represent the oscillatory trajectory along a line in the direction  $(-1,-1,-1)$  in the Bloch-vector space. In (a) the trajectory hits the origin in a finite time while in (b) it approaches the origin asymptotically.

## V. CONCLUSIONS

The time evolution of quantum entanglement and quantum discord in 2-qubit systems behave in fundamentally different ways. For the most part, this difference comes from the different topologies of the zero sets: the set of separable states and the set of concordant states, respectively. The set of separable states is a convex 15-manifold. The set of concordant states is a non-convex simply-connected when a certain set of zero measure has been subtracted out. The generic time evolutions for the disappearance of entanglement are of the E and O types, with A and B possible for symmetric situations. The generic evolutions for discord disappearance are of A and B types, but discord disappearance depends on having the asymptotic limit point lie on a set of low dimension:

Entanglement	A	E	B	O
Discord	A		B	
Joint evolutions	AA	EA, EB	BB	OB

TABLE II: Possible Routes for Disappearance of Entanglement and Discord in Physical Systems. This table summarizes the possible ways that entanglement and discord can disappear in physics models. Each joint evolution corresponds to a different topology of two sets: the intersections of the system trajectory with  $\mathcal{S}$ , the set of separable states, and with  $\mathcal{C}$ , the set of concordant states. We do not include pathological trajectories with discontinuous derivatives or highly symmetrical models whose trajectories are confined to low-dimensional submanifolds.

it is more rare than entanglement disappearance, but it happens naturally in physical models, since, for example, the completely mixed state is a common limit point. E and O types of behavior are not allowed for discord. Furthermore, there are coexistence rules for joint evolution. All these facts are summarized in the following table. The time evolution of quantum entanglement and quantum discord in 2-qubit systems behave in fundamentally different ways. For the most part, this difference comes from the different topologies of the zero sets: the set of separable states and the set of concordant states, respectively. The set of separable states is a convex 15-manifold. The set of concordant states is a non-convex simply-connected 9-manifold when certain sets of zero measure have been subtracted out. The generic time evolutions for the disappearance of the entanglement are of the E and O types, with A and B possible for highly symmetric situations. The generic evolution of discord disappearance is of A and B types, but discord disappearance depends on having the asymptotic limit point lie on a set of low dimension, so it is more rare than entanglement disappearance. E and O type of behavior do not occur. Roszak *et al.* have computed the joint evolution of entanglement and geometric discord in a model of two excitonic quantum dot qubits dephased by noise from phonons<sup>22</sup>. They find the expected phenomenon of incomplete disappearance of discord at long times when the temperature is finite (and therefore the final state is not fully mixed.) This case is not included in our analysis, though the generalization is straightforward. In cases where the disappearance is complete, they observe EA and EB behaviors for this model. Benedetti *et al.* have done similar calculations for two qubits subjected to classical noise<sup>23</sup>. They observe OB and BB behavior, except when considering models that produce trajectories confined to a low-dimensional manifold - in their case a mixture of Bell states.

Once the topology of the zero set is understood, the construction of explicit models that display the various behaviors is relatively straightforward. In particular one can show that qualitatively different behaviors of entanglement and discord can be observed in the same system.

This is true even if the evolution is unitary: with an Ising interaction one can find oscillatory behavior of the discord even though the entanglement is strictly zero at all times, for a judicious choice of the initial state. With a slightly more complicated Hamiltonian still with unitary time development of the state, the coexistence of all reversible types of oscillatory evolution for entanglement and discord can be obtained. For example, B or bouncing behavior of the discord is compatible with the O-type behavior of the concurrence in which the state is separable for an infinite number of finite time intervals. For non-unitary evolution, it is also found that all different kinds of evolutions of discord and entanglement can coexist. We are able to produce coexistence of A (half-life) type behavior of the discord with E-type (entanglement sudden death), as well as A behavior for both; coexistence of the various kinds of decaying oscillatory behavior is also possible.

It is not difficult to see how these evolutions correlate with various topologies of the intersections of the state trajectory and the zero sets. For these considerations, the difference between different measures of entanglement and the difference between geometric and quantum discord is not material. For the question of frozen discord, however, the distinction between geometric and quantum discord is essential. Frozen discord occurs, by definition, when the trajectory is along a line of constant discord. Since discord is unrelated to dynamics, this can

occur (in the absence of fine tuning) only when both the trajectory and the discord are constrained by symmetry. Symmetry constraints typically lead to straight-line trajectories. The surfaces of constant discord are not flat, while the surfaces of constant geometric discord can be. Accordingly, we only see frozen *geometric* discord only in situations with high symmetry, and frozen *quantum* discord does not occur in natural models.

## VI. ACKNOWLEDGMENTS

This work is supported by DARPA QuEST program, Grant No. MSN118850. We thank Hyungjun Lim for useful discussions.

### Appendix A: The Bloch vector of a concordant state

In this section, we obtain the 15 components of the Bloch vector for a concordant state. We define two projection operators:  $\Pi_k \equiv |\Psi_k\rangle\langle\Psi_k| = \frac{1}{2}(\sigma_0 \pm \vec{n}_k \cdot \vec{\sigma})$  where  $\vec{n}_k \equiv (n_{1k}, n_{2k}, n_{3k}) = (\sin\theta \cos\varphi, \sin\theta \sin\varphi, \cos\theta)$  is a Bloch unit vector. Qubit B is  $\rho_k = \frac{1}{2}(\sigma_0 \pm \vec{n}_k \cdot \vec{\sigma})$ . We can rewrite Eq. (4) using these notations and the generalized Bloch vector becomes:

$$N_{ij} = \frac{p}{2}\text{Tr}(\Pi_0 \otimes \sigma_0)(\sigma_i \otimes \sigma_j) + \frac{1-p}{2}\text{Tr}(\Pi_1 \otimes \sigma_0)(\sigma_i \otimes \sigma_j) + \quad (\text{A1})$$

$$\begin{aligned} & + \frac{p}{2} \sum_{k=1}^3 n_{0k} \text{Tr}(\Pi_0 \otimes \sigma_k)(\sigma_i \otimes \sigma_j) + \frac{1-p}{2} \sum_{k=1}^3 n_{1k} \text{Tr}(\Pi_1 \otimes \sigma_k)(\sigma_i \otimes \sigma_j) \\ & = p\delta_{j,0} \text{Tr}\Pi_0\sigma_i + (1-p)\delta_{j,0} \text{Tr}\Pi_1\sigma_i \\ & \quad + p(1-\delta_{j,0})n_{0j} \text{Tr}\Pi_0\sigma_i + (1-p)(1-\delta_{j,0})n_{1j} \text{Tr}\Pi_1\sigma_i. \\ \Leftrightarrow N_{ij} & = p[\delta_{j,0} + (1-\delta_{j,0})n_{0j}] \text{Tr}\Pi_0\sigma_i + (1-p)[\delta_{j,0} + (1-\delta_{j,0})n_{1j}] \text{Tr}\Pi_1\sigma_i. \quad (\text{A2}) \end{aligned}$$

These results can then be used to obtain the explicit forms for  $N_{ij}$  given in (5), (6), and (7) of the main text.

### Appendix B: Concordant states on the coordinate axes

We wish to show that  $\mathcal{C}$  contains the coordinate axes.

$$\begin{aligned} \rho & = \frac{1}{4}(\sigma_0 \otimes \sigma_0 + \sum_i N_{0i} \sigma_0 \otimes \sigma_i) \\ & = \left(\frac{1}{2}\sigma_0\right) \otimes \frac{1}{2}\left(\sigma_0 + \sum_i N_{0i}\sigma_i\right) \\ & = \frac{1}{2}\Pi_0 \otimes \rho_0 + \frac{1}{2}\Pi_1 \otimes \rho_0 \quad (\text{B1}) \end{aligned}$$

where  $\Pi_i; i = 0, 1$  form an orthonormal basis in qubit A while  $\rho_0 = \frac{1}{2}(\sigma_0 + \sum_i N_{0i}\sigma_i)$  is a general state of qubit B given  $N_{0i} \in [-1, 1]$ . This is always satisfied using the condition of positivity for system qubit  $\rho$ . The last line in Eq. (B1) is the necessary and sufficient condition for state  $\rho$  to be concordant.

### Appendix C: Symmetries in the concordant subset

Generally, concordant states are asymmetric under exchange of the two qubits. In this appendix, we show that a concordant state is symmetric under some certain conditions. The left 0-discord state has the Bloch vector described

as in Eqs. (5), (6), (7) and “left” geometric discord as in (3) where

$$\begin{aligned} k_{\max} &= \sum_{i=1}^3 N_{i0}^2 + \sum_{i,j=1}^3 N_{ij}^2 \\ &= |\underline{N}|^2 - (N_{01}^2 + N_{02}^2 + N_{03}^2). \end{aligned} \quad (\text{C1})$$

A “right” 0-ddiscord state, instead, has:

$$\begin{aligned} N'_{0i} &= (2p' - 1)m'_i \\ N'_{i0} &= p' n'_{0i} + (1 - p')n'_{1i} \\ N'_{ij} &= m'_i[p' n'_{0j} - (1 - p')n'_{1j}] \end{aligned} \quad (\text{C2})$$

and its “right” geometric discord is

$$\mathcal{D}_G^R = \frac{1}{4}[\text{Tr}(\vec{y}\vec{y}^T) + \text{Tr}(\mathcal{T}'\mathcal{T}'^T) - q_{\max}]$$

where  $\vec{y}^T = (N'_{10}, N'_{20}, N'_{30})$  and  $q_{\max}$  is the largest eigenvalues of  $\vec{y}\vec{y}^T + \mathcal{T}'\mathcal{T}'^T$ . Generally, a left concordant state has  $\mathcal{D}_G^R \neq 0$ . Now, we discuss several cases which have  $\mathcal{D}_G^L = 0 = \mathcal{D}_G^R$  i.e. symmetric concordant states. If a (left) concordant state has  $N_{0i} = \pm N_{i0}$ , which is equivalent to the condition  $p\vec{n}_0 + (1-p)\vec{n}_1 = \pm(2p-1)\vec{m}$ , then it is symmetric. Typical symmetric concordant point is the origin which has  $p = 1/2$  and  $\vec{n}_i = \vec{0}$ . All pure concordant states satisfying two conditions  $p(1-p) = 0$  &  $|\vec{n}_0||\vec{n}_1| = 1$  are also symmetric.

#### Appendix D: Linear independence of the tangent vectors

We obtain the explicit form for the 9 tangent vectors to the manifold  $\mathcal{C}$  as follows:

$$\vec{t}_1 = \frac{\partial \vec{N}}{\partial \theta} = \vec{0} + (2p-1) \sum_{i=1}^3 \frac{\partial m_i}{\partial \theta} \vec{e}_{i0} + \sum_{i,j=1}^3 [pn_{0j} - (1-p)n_{1j}] \frac{\partial m_i}{\partial \theta} \vec{e}_{ij} \quad (\text{D1a})$$

$$\vec{t}_2 = \frac{\partial \vec{N}}{\partial \varphi} = \vec{0} + (2p-1) \sum_{i=1}^3 \frac{\partial m_i}{\partial \varphi} \vec{e}_{i0} + \sum_{i,j=1}^3 [pn_{0j} - (1-p)n_{1j}] \frac{\partial m_i}{\partial \varphi} \vec{e}_{ij} \quad (\text{D1b})$$

$$\vec{t}_3 = \frac{\partial \vec{N}}{\partial p} = \sum_{i=1}^3 (n_{0i} - n_{1i}) \vec{e}_{0i} + 2 \sum_{i=1}^3 m_i \vec{e}_{i0} + \sum_{i,j=1}^3 m_i (n_{0j} - n_{1j}) \vec{e}_{ij} \quad (\text{D1c})$$

$$\vec{t}_4 = \frac{\partial \vec{N}}{\partial n_{01}} = p \sum_{i=1}^3 \delta_{i,1} \vec{e}_{0i} + \vec{0} + p \sum_{i=1}^3 m_i \delta_{j,1} \vec{e}_{ij} \quad (\text{D1d})$$

$$\vec{t}_5 = \frac{\partial \vec{N}}{\partial n_{02}} = p \sum_{i=1}^3 \delta_{i,2} \vec{e}_{0i} + \vec{0} + p \sum_{i=1}^3 m_i \delta_{j,2} \vec{e}_{ij} \quad (\text{D1e})$$

$$\vec{t}_6 = \frac{\partial \vec{N}}{\partial n_{03}} = p \sum_{i=1}^3 \delta_{i,3} \vec{e}_{0i} + \vec{0} + p \sum_{i=1}^3 m_i \delta_{j,3} \vec{e}_{ij} \quad (\text{D1f})$$

$$\vec{t}_7 = \frac{\partial \vec{N}}{\partial n_{11}} = (1-p) \sum_{i=1}^3 \delta_{i,1} \vec{e}_{0i} + \vec{0} - (1-p) \sum_{i=1}^3 m_i \delta_{j,1} \vec{e}_{ij} \quad (\text{D1g})$$

$$\vec{t}_8 = \frac{\partial \vec{N}}{\partial n_{12}} = (1-p) \sum_{i=1}^3 \delta_{i,2} \vec{e}_{0i} + \vec{0} - (1-p) \sum_{i=1}^3 m_i \delta_{j,2} \vec{e}_{ij} \quad (\text{D1h})$$

$$\vec{t}_9 = \frac{\partial \vec{N}}{\partial n_{13}} = (1-p) \sum_{i=1}^3 \delta_{i,3} \vec{e}_{0i} + \vec{0} - (1-p) \sum_{i=1}^3 m_i \delta_{j,3} \vec{e}_{ij}. \quad (\text{D1i})$$

The tensor matrix has explicit form as:

$$g = \begin{pmatrix} g_{11} & 0 & 0 & 0 & 0 & 0 & 0 & 0 & 0 \\ 0 & g_{22} & 0 & 0 & 0 & 0 & 0 & 0 & 0 \\ 0 & 0 & g_{33} & g_{34} & g_{35} & g_{36} & 0 & 0 & 0 \\ 0 & 0 & g_{43} & g_{44} & 0 & 0 & 0 & 0 & 0 \\ 0 & 0 & g_{53} & 0 & g_{55} & 0 & 0 & 0 & 0 \\ 0 & 0 & g_{63} & 0 & 0 & g_{66} & 0 & 0 & 0 \\ 0 & 0 & 0 & 0 & 0 & 0 & g_{77} & 0 & 0 \\ 0 & 0 & 0 & 0 & 0 & 0 & 0 & g_{88} & 0 \\ 0 & 0 & 0 & 0 & 0 & 0 & 0 & 0 & g_{99} \end{pmatrix}$$

with  $g_{11} = (1-2p)^2 + \sum_{i=1}^3 [pn_{0i} - (1-p)n_{1i}]^2$ ;  $g_{22} = \{(1-2p)^2 + \sum_{i=1}^3 [pn_{0i} - (1-p)n_{1i}]^2\} \sin^2 \theta$ ;  $g_{33} = 2[2 + \sum_{i=1}^3 (n_{0i} - n_{1i})^2]$ ;  $g_{44} = g_{55} = g_{66} = 2p^2$ ;  $g_{77} = g_{88} = g_{99} = 2(1-p)^2$ ;  $g_{34} = g_{43} = 2p(n_{01} - n_{11})$ ;  $g_{35} = g_{53} = 2p(n_{02} - n_{12})$ ;  $g_{36} = g_{63} = 2p(n_{03} - n_{13})$ .

**Appendix E: Quantum discord of the state in Eq. (17)**

The corresponding density matrix  $\rho(t) = \frac{1}{4}(\sigma_0 \otimes \sigma_0 + S_3\sigma_1 \otimes \sigma_3 + C_3\sigma_2 \otimes \sigma_0)$  has 4 eigenvalues of  $\{\frac{1}{2}, \frac{1}{2}, 0, 0\}$  and  $S[\rho(t)] = 1$ . The two subsystems are:  $\rho_A(t) = \frac{1}{2} \begin{pmatrix} 1 & -iC_3 \\ iC_3 & 1 \end{pmatrix}$  with two eigenvalues  $\lambda_A = \frac{1}{2}(1 \pm C_3)$ ; and  $\rho_B(t) = \sigma_0/2$ .

The quantum mutual information is:

$$\begin{aligned} \mathcal{I} &= S[\rho_A(t)] + S[\rho_B(t)] - S[\rho(t)] \\ &= S[\rho_A(t)] \\ &= 1 - \frac{1}{2}[(1 - C_3) \log(1 - C_3) \\ &\quad + (1 + C_3) \log(1 + C_3)]. \end{aligned} \quad (\text{E1})$$

The classical mutual information is

$$\begin{aligned} \mathcal{J}^{\text{class}} &= S[\rho_B(t)] - \min_{\{A_k\}} S[\rho(t)|A_k] \\ &= 1 - \min_{\{A_k\}} S[\rho(t)|A_k] \end{aligned} \quad (\text{E2})$$

where  $\{A_k = V\Pi_k V^\dagger; k = 1, 2\}$  defines a set of measurement on subsystem A:  $V = t\sigma_0 + \vec{v} \cdot \vec{\sigma}$  where  $t^2 + v_1^2 + v_2^2 + v_3^2 = 1$  and  $\{\Pi_k\}$  is some local orthogonal basis. Without loss of generality, we choose  $\Pi_1 = \begin{pmatrix} 1 & 0 \\ 0 & 0 \end{pmatrix}$  and  $\Pi_2 = \begin{pmatrix} 0 & 0 \\ 0 & 1 \end{pmatrix}$ . Some useful expressions are used:  $\Pi_1\sigma_i\Pi_1 = \delta_{i,3}\Pi_1$ ;  $\Pi_2\sigma_i\Pi_2 = -\delta_{i,3}\Pi_2$ ,

$$z_1 = \text{Tr}V^\dagger\sigma_1V\sigma_3 = 2(-tv_2 + v_1v_3), \quad (\text{E3})$$

$$z_2 = \text{Tr}V^\dagger\sigma_2V\sigma_3 = 2(tv_1 + v_2v_3), \quad (\text{E4})$$

$$z_3 = \text{Tr}V^\dagger\sigma_3V\sigma_3 = t^2 + v_3^2 - v_1^2 - v_2^2. \quad (\text{E5})$$

After measurement  $\{A_k\}$  the system is sent to  $\rho_k(t) = \frac{A_k\rho(t)A_k}{\text{Tr}(A_k\rho(t)A_k)}$ . Set  $p_k = \text{Tr}(A_k\rho(t)A_k)$  with  $p_1 = \frac{1+X}{2}, p_2 = \frac{1-X}{2}$  where  $X = 2C_3(tv_1 + v_2v_3) = z_2C_3$ , one obtains:

$$\begin{aligned} p_1\rho_1(t) &= A_1\rho(t)A_1 \\ &= \frac{1}{4}(V \otimes \sigma_0)(\Pi_1 \otimes \sigma_0) \\ &\quad (V^\dagger \otimes \sigma_0)(\sigma_0 \otimes \sigma_0 + C_3\sigma_2 \otimes \sigma_0 + S_3\sigma_1 \otimes \sigma_3)(V \otimes \sigma_0) \\ &\quad (\Pi_1 \otimes \sigma_0)(V^\dagger \otimes \sigma_0) \\ p_1\rho_1(t) &= \frac{1}{4}(V\Pi_1V^\dagger) \otimes [(1+X)\sigma_0 + Y\sigma_3] \end{aligned} \quad (\text{E6})$$

with X defined above and  $Y = z_1S_3$ .

Similarly,  $\rho_2(t)$  is obtained as:

$$p_2\rho_2(t) = (V\Pi_1V^\dagger) \otimes [(1-X)\sigma_0 - Y\sigma_3]. \quad (\text{E7})$$

Now, eigenvalues of  $\rho_1(t)$  are  $\frac{1}{4p_1}(1+X+Y); \frac{1}{4p_1}(1+X-Y)$  and of  $\rho_2(t)$  are  $\frac{1}{4p_2}(1-X+Y); \frac{1}{4p_2}(1-X-Y)$ . One can obtain the conditional entropy as:

$$\begin{aligned} S[\rho(t)|A_k] &= p_1S[\rho_1(t)] + p_2S[\rho_2(t)] \\ &= 1 - \frac{1}{4}[(1+X+Y) \log(1+X+Y) + (1+X-Y) \log(1+X-Y) \\ &\quad + (1-X+Y) \log(1-X+Y) + (1-X-Y) \log(1-X-Y) \\ &\quad - 2(1+X) \log(1+X) - 2(1-X) \log(1-X)]. \end{aligned} \quad (\text{E8})$$

Note that  $X = 2C_3(tv_1 + v_2v_3) \leq |C_3|$ ;  $Y = 2S_3(-tv_2 + v_1v_3) \leq |S_3|$ . (E8) has identical minima at  $X = 0$  &

$Y = \pm S_3$ . As a result,

$$\begin{aligned} \min_{\{A_k\}} S[\rho(t)|A_k] &= 1 - \frac{1}{2}[(1 - |S_3|) \log(1 - |S_3|) \\ &\quad + (1 + |S_3|) \log(1 + |S_3|)] \end{aligned} \quad (\text{E9})$$

Now substitute (E9) into (E2) and subtract (E2) from (E1) the quantum discord is obtained as in the main text.

### Appendix F: Quantum discord of the state in Eq. (34)

Note that

$$\begin{aligned} |\vec{N}(t)| &= \sqrt{N_{20}^2(t) + N_{13}^2(t)} \\ &= e^{-\gamma t} \left| \cosh(2iR_0 t) - i \frac{\gamma}{2R_0} \sinh(2iR_0 t) \right|. \end{aligned} \quad (\text{F1})$$

Entropy of the system (34) is

$$S_\rho = -(\lambda_1 \log \lambda_1 + \lambda_2 \log \lambda_2 + \lambda_3 \log \lambda_3 + \lambda_4 \log \lambda_4) \quad (\text{F2})$$

where

$$\begin{aligned} \lambda_{1,2} &= \frac{1}{4} [1 + \sqrt{N_{20}^2(t) + N_{13}^2(t)}] \\ \lambda_{3,4} &= \frac{1}{4} [1 - \sqrt{N_{20}^2(t) + N_{13}^2(t)}]. \end{aligned} \quad (\text{F3})$$

Entropy of system A is

$$S_{\rho_A} = 1 - \frac{1}{2} \{ [1 + N_{20}(t)] \log [1 + N_{20}(t)] + [1 - N_{20}(t)] \log [1 - N_{20}(t)] \} \quad (\text{F4})$$

and the classical mutual information after optimization is:

$$S_{\text{class.}} = 1 - \frac{1}{2} \{ [1 + N_{13}(t)] \log [1 + N_{13}(t)] + [1 - N_{13}(t)] \log [1 - N_{13}(t)] \}. \quad (\text{F5})$$

The time evolution of the quantum discord of the above system:  $\mathcal{D}(t) = S_{\rho_A} - S_\rho + S_{\text{class.}}$ .

### Appendix G: Quantum discord of the state in Eq. (36)

$$\begin{aligned} \mathcal{D}(t) &= 2 - \frac{1+\alpha}{2} \log(1+\alpha) - \frac{1-\alpha}{2} \log(1-\alpha) \\ &\quad - S_\rho \end{aligned} \quad (\text{G1})$$

where  $S_\rho = -\lambda_0 \log \lambda_0 - \lambda_1 \log \lambda_1 - \lambda_2 \log \lambda_2 - \lambda_3 \log \lambda_3$  with  $\lambda_0 = \lambda_1 = \frac{1-\alpha}{4}$ ;  $\lambda_{2,3} = \frac{1+\alpha \pm 2\sqrt{N_{11}^2(t) + N_{12}^2(t)}}{4}$ .

### Appendix H: Quasi-Hamiltonian $H_q$ of the XY-model

This section is for further discussions of solving the XY-model in a non-unitary evolution.

In a general XY-model in interaction with a single RTN fluctuator ( $B_z = 0$ ),  $H_q$  has 15 different eigenvalues:  $-2i\gamma, -i\gamma, -2R_0, -i\gamma \pm 2R_0, -i\gamma \pm W_1, -i\gamma \pm W_2, \omega_1, \omega_2, \omega_3, \Omega_1, \Omega_2, \Omega_3$  where  $W_{1,2} = \sqrt{4J_{yx}^2 + 2g_z^2 - \gamma^2 \pm \sqrt{g_z^4 + 4J_{yx}^2 g_z^2 - 4J_{yx}^2 \gamma^2}}$ ;  $\omega_i$  and  $\Omega_i$ , respectively, are roots of polynomial  $-32J_{yx}^2 - 4(4J_{yx}^2 + g_z^2)\omega + 2i\gamma\omega^2 + \omega^3$  and  $-8ig_z^2\gamma - 4(4J_{yx}^2 + g_z^2 + \gamma^2)\Omega + 4i\gamma\Omega^2 + \Omega^3$ .

### Appendix I: Analytical solution of two uncorrelated RTN fluctuators with different transition rates $\gamma, \xi\gamma$

We obtain exact solutions for the Ising models in interaction with two different uncorrelated noise sources. For the components constructing a general off- $\mathbf{X}$ -type of class [see the left-hand-side (LHS) of Eqs. (15) and (16)], the solution yields by replacing  $\gamma$  as in the single fluctuator case [see Eq. (34)] by  $\gamma_1, \gamma_2$  (respectively, equals  $\gamma, \xi\gamma$ ) for the corresponding subclass. It is due to the fact that the LHS components in Eq. (15) commute with the term  $\sigma_0 \otimes \sigma_3$  and the LHS components in Eq. (16) commute with the term  $\sigma_3 \otimes \sigma_0$ . As a result, each subclass is not affected by the noise from the other qubit. More generally, if a Hamiltonian consists of  $k$  commute terms then the combined solution is  $N_{ij}(t) = \sum_{i,j} N_{ij} \Pi_{m=1}^k f_{ij}^m(t)$  where  $\sum_{i,j} N_{ij} f_{ij}^m(t)$  is the solution for the  $m$ -th term. Back to the above case, one has:

$$\begin{aligned} N_{01}(t) &= (N_{01}C_3 + N_{32}S_3)e^{-\xi\gamma t} F(R_2) \\ N_{32}(t) &= (N_{32}C_3 - N_{01}S_3)e^{-\xi\gamma t} F(R_2) \\ N_{02}(t) &= (N_{30}C_3 - N_{31}S_3)e^{-\xi\gamma t} F(R_2) \\ N_{31}(t) &= (N_{31}C_3 + N_{02}S_3)e^{-\xi\gamma t} F(R_2); \end{aligned} \quad (\text{I1})$$

$$\begin{aligned} N_{10}(t) &= (N_{10}C_3 + N_{23}S_3)e^{-\gamma t} F(R_1) \\ N_{23}(t) &= (N_{23}C_3 - N_{10}S_3)e^{-\gamma t} F(R_1) \\ N_{20}(t) &= (N_{03}C_3 - N_{13}S_3)e^{-\gamma t} F(R_1) \\ N_{13}(t) &= (N_{13}C_3 + N_{20}S_3)e^{-\gamma t} F(R_1) \end{aligned} \quad (\text{I2})$$

where  $R_{1,2} = \sqrt{4g_z^2 - \gamma_{1,2}^2}/2$ .

The enhanced noise effect will be seen in the other class - the  $\mathbf{X}$ -type:

$$\begin{aligned} N_{ij}(t) &= N_{ij} e^{-\gamma(1+\xi)t} H(R_0, \xi), \quad i, j = 1 \div 3 \\ N_{33}(t) &= N_{33} \end{aligned} \quad (\text{I3})$$

where

$$\begin{aligned} H(R_0, \xi) &= \frac{1}{4R_0 X_0} [2R_0 \cosh(2iR_0 t) - i\gamma \sinh(2iR_0 t)] \\ &\quad [2X_0 \cosh(2iX_0 t) - i\xi\gamma \sinh(2iX_0 t)]. \end{aligned} \quad (\text{I4})$$

Here,  $X_0 = \sqrt{4R_0^2 - \gamma^2(\xi^2 - 1)}/2$ . If  $\xi = 1$  (i.e.  $\gamma_1 = \gamma_2$ ) then  $X_0=R_0$  and  $H(R_0, \xi) \equiv G(R_0)$  as defined in (40).

- 
- <sup>1</sup> E. Schrödinger, Proc. Cambridge Philos. Soc. **31**, 555 (1935).  
<sup>2</sup> L. Henderson and V. Vedral, J. Phys. A **34**, 6899 (2001).  
<sup>3</sup> H. Ollivier and W. H. Zurek, Phys. Rev. Lett. **88**, 017901 (2001).  
<sup>4</sup> E. Knill and R. Laflamme, Phys. Rev. Lett. **81**, 5672 (1998).  
<sup>5</sup> A. Datta, S. T. Flammia, and C. M. Caves, Phys. Rev. A **72**, 042316 (2005).  
<sup>6</sup> A. Datta, A. Shaji, and C. M. Caves, Phys. Rev. Lett. **100**, 050502 (2008).  
<sup>7</sup> C.H. Bennett and S.J. Wiesner, Phys. Rev. Lett. **69**, 2881 (1992).  
<sup>8</sup> K. Modi, A. Brodutch, H. Cable, T. Paterek, and V. Vedral, Rev. Mod. Phys. **84**, 1655 (2012).  
<sup>9</sup> T. Yu and J. H. Eberly, Science **323**, 598 (2009).  
<sup>10</sup> T. Werlang, S. Souza, F. F. Fanchini, and C. J. Villas Boas, Phys. Rev. A **80**, 024103 (2009).  
<sup>11</sup> L. Mazzola, J. Piilo, and S. Maniscalco, Phys. Rev. Lett. **104**, 200401 (2010).  
<sup>12</sup> A. Ferraro, L. Aolita, D. Cavalcanti, F. M. Cucchietti, and A. Acín, Phys. Rev. A **81**, 052318 (2010).  
<sup>13</sup> F. F. Fanchini, T. Werlang, C. A. Brasil, L. G. E. Arruda, and A. O. Caldeira, Phys. Rev. A **81**, 052107 (2010).  
<sup>14</sup> F. F. Fanchini, L. K. Castelano, and A. O. Caldeira, New J. Phys. **12**, 073009 (2010).  
<sup>15</sup> M. D. Lang, C. C. Caves, and A. Shaji, Int. J. Quantum Inform. **9**, 1553 (2011).  
<sup>16</sup> L. Mazzola, J. Piilo, and S. Maniscalco, Int. J. Quantum Inform. **9**, 981 (2011).  
<sup>17</sup> B. Bellomo, R. Lo Franco, and G. Compagno, Phys. Rev. A **86**, 012312 (2012).  
<sup>18</sup> A. K. Pal and I. Bose, Eur. Phys. J. B **85**, 277 (2012).  
<sup>19</sup> D. Zhou and R. Joynt, Quantum Inf. Process **11**, 571 (2012).  
<sup>20</sup> D. Zhou, G. W. Chern, J. Fei, and R. Joynt, Int. J. Mod. Phys. B **26**, 1250054 (2012).  
<sup>21</sup> M. D. Lang and C. M. Caves, Phys. Rev. Lett. **105**, 150501 (2010).  
<sup>22</sup> K. Roszak, P. Mazurek, and P. Horodecki, Phys. Rev. A **87**, 062308 (2013).  
<sup>23</sup> C. Benedetti, F. Buscemi, P. Bordone, and M. Paris, Phys. Rev. A **87**, 052328 (2013).  
<sup>24</sup> S. Luo, Phys. Rev. A **77**, 042303 (2008).  
<sup>25</sup> M. Ali, A. R. P. Rau, and G. Alber, Phys. Rev. A **81**, 042105 (2010).  
<sup>26</sup> D. Girolami and G. Adesso, Phys. Rev. A **83**, 052108 (2011); Phys. Rev. A **84**, 052110 (2011).  
<sup>27</sup> B. Dakić, V. Vedral, and C. Brukner, Phys. Rev. Lett. **105**, 190502 (2010).  
<sup>28</sup> D. Girolami and G. Adesso, Phys. Rev. Lett. **108**, 150403 (2012).  
<sup>29</sup> L. Jakóbczyk and M. Siennicki, Phys. Lett. A **286**, 383 (2001).  
<sup>30</sup> S. Luo and S. Fu, Phys. Rev. A **82**, 034302 (2010).  
<sup>31</sup> H. Lim and R. Joynt (in preparation).  
<sup>32</sup> C. H. Bennett, D. P. DiVincenzo, J. Smolin, and W. K. Wootters, Phys. Rev. A **54**, 3824 (1996).  
<sup>33</sup> W. K. Wootters, Phys. Rev. Lett. **80**, 2245 (1998).  
<sup>34</sup> R. F. Werner, Phys. Rev. A **40**, 4277 (1989).  
<sup>35</sup> B. Cheng, Q. H. Wang, and R. Joynt, Phys. Rev. A **78**, 022313 (2008).  
<sup>36</sup> R. Joynt, D. Zhou, and Q. H. Wang, Int. J. Mod. B **25**, 2115 (2011); D. Zhou and R. Joynt, Phys. Rev. A **81**, 010103 (2010).  
<sup>37</sup> D. A. Lidar, I. L. Chuang, and K. B. Whaley, Phys. Rev. Lett. **81**, 2594 (1998).